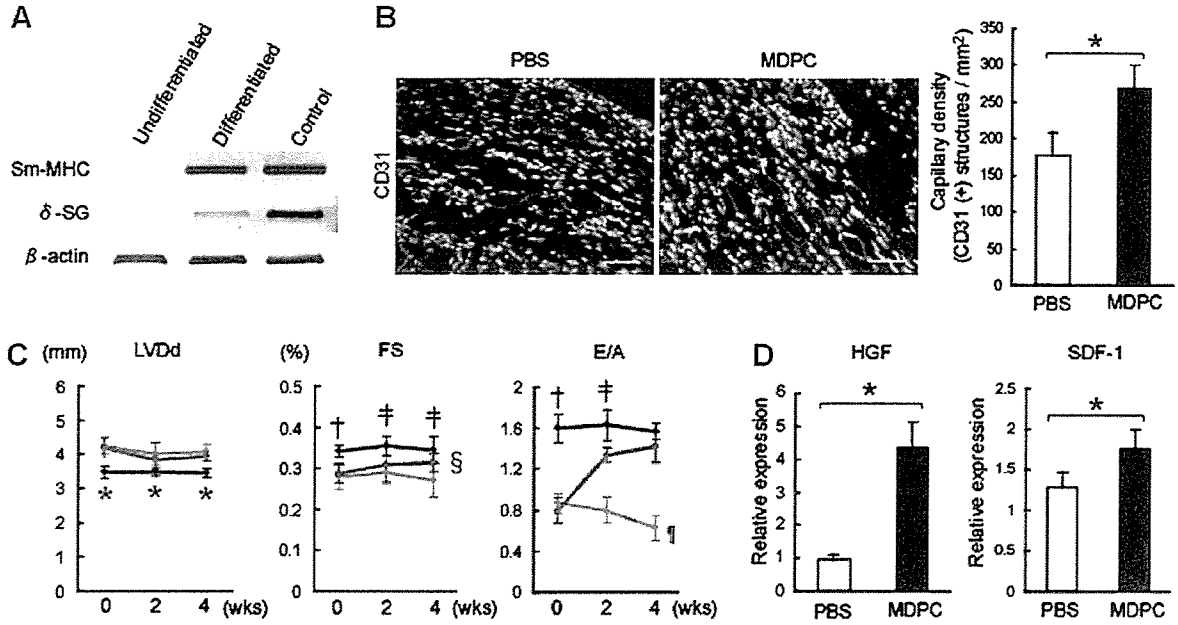

Fig. 4. MDPC transplantation improves cardiac function partially through paracrine effectors production (A) δ-SG expression was observed in differentiated MDPCs in vitro. (B) Comparison of the capillary density between PBS-treated and MDPC-transplanted δ-SG KD hearts. CD31 (red). DAPI (blue). $^{*}p < 0.01$. (C) The effect of MDPC transplantation in δ-SG KD hearts shown by echocardiograms. Black lines: NTG mice. Blue lines: PBS-treated group. Red lines: MDPC-transplanted group. $^{*}p < 0.05$; $^{\dagger}p < 0.01$ vs. PBS- and MDPC-treated mice. $^{\ddagger}p < 0.01$ vs. PBS-injected mice and $p < 0.05$ vs. MDPC-transplanted mice. $^{\S}p < 0.05$ vs. PBS-injected mice. $^{\P}p < 0.01$ vs. NTG and MDPC-treated mice compared with the same time point. (D) Relative gene expression for HGF and SDF-1 was measured by real-time RT-PCR. $^{*}p < 0.01$. Scale bars represent 50 μm in (B).

they might be reminiscent of mesenchymal cells derived from perivascular cells (PVCs) [18] or mesoangioblasts that are putative ancestors of PVCs [19], which can be classified as pericytes in capillaries and are essential for the development of functional vessel walls. Because PVCs are thought to have the potential to regenerate mesenchymal cells, MDPCs may reflect in some aspects of the phenotype of MSCs originally isolated from bone marrow stroma.

Previous report demonstrated that BM-SP cells could be engrafted in δ-SG null hearts, but failed to restore the δ-SG expression [15]. The absence of δ-SG expression after transplantation suggested that cellular fusion, as opposed to de novo differentiation, occurred with transplanted BM-SP cells which led to impaired maturation of implanted cells. In contrast, we observed that transplanted MDPCs did differentiate into mature vascular cells with the restoration of δ-SG expression, indicating autonomous vascular-differentiation might occur after MDPC transplantation.

It is important to determine whether local intramuscular injection of MDPCs into δ-SG KD heart is sufficient to deliver the cells into focally degenerated lesions and contributes to functional recovery. We observed extensive angiogenesis induced by MDPC transplantation to achieve a better preservation of cardiac function. However, the lack of improvement in diastolic dimension did not favor a scaffolding effect of the grafted MDPCs in δ-SG KD hearts similar to the previous report [20]. In our study, engrafted MDPCs were incorporated mostly into vascular cells, but muscular regeneration was rarely observed. One of the reasons is that δ-SG KD mice showed a predominantly lower expression of δ-SG along vascular smooth muscle cells, as previously reported [21], leading to scarce muscular artery and particularly extensive fibrosis surrounding the vessels. This focal defect in the δ-SG KD heart might be one of the causes for transplanted MDPCs to differentiate into vascular cells more efficiently than into cardiac or skeletal muscle fibers.

Our results also suggested that transplanted MDPCs could induce the secretion of HGF and SDF-1, that is consistent with the recent reports demonstrating that HGF could promote stem cell activation and reduced cardiomyocyte apoptosis in the myocardium of δ-SG-null hamsters [22], and that SDF-1 was sufficient to induce therapeutic stem cell homing to injured myocardium [23]. Taken together, the beneficial effects of MDPC transplantation might be due to increased blood supply produced by angiogenesis and promoted secretion of specific growth factors, leading to modulation of adverse LV remodeling and improvement of cardiac function.

In conclusion, transplantation of MDPCs induced substantial angiogenesis and increased secretion of paracrine mediators, resulting in the improvement of cardiac function in δ-SG KD mice. Our findings indicate that MDPCs may be the promising progenitor cells in adult skeletal muscle for cell therapy to treat δ-sarcoglycan complex mutant cardiomyopathy.

Acknowledgments

We thank the investigators cited for generously donating plasmids: S. Ishii, and M. Imamura; Y. Yoshida, A. Kosugi, and M. Nishikawa for technical assistance. This work was supported by Grants-in-Aid from the Ministry of Education, Culture, Sports, Science and Technology of Japan, and by Grants-in-Aid from the Ministry of Health, Labor, and Welfare of Japan.

References

[1] C.A. Collins, I. Olsen, P.S. Zammit, L. Heslop, A. Petrie, T.A. Partridge, J.E. Morgan, Stem cell function, self-renewal, and behavioral heterogeneity of cells from the adult muscle satellite cell niche, Cell 122 (2005) 289–301.

[2] I.W. McKinnell, G. Parise, M.A. Rudnicki, Muscle stem cells and regenerative myogenesis, Curr. Top Dev. Biol. 71 (2005) 113–130.

[3] N. Hashimoto, T. Murase, S. Kondo, A. Okuda, M. Inagawa-Ogashiwa, Muscle reconstitution by muscle satellite cell descendants with stem cell-like properties, Development 131 (2004) 5481–5490.

[4] Z. Qu-Petersen, B. Deasy, R. Jankowski, M. Ikezawa, J. Cummins, R. Pruchnic, J. Mytinger, B. Cao, C. Gates, A. Wernig, J. Huard, Identification of a novel population of muscle stem cells in mice: potential for muscle regeneration, J. Cell Biol. 157 (2002) 851–864.

[5] H. Oshima, T.R. Payne, K.L. Urish, T. Sakai, Y. Ling, B. Gharaibeh, K. Tobita, B.B. Keller, J.H. Cummins, J. Huard, Differential myocardial infarct repair with muscle stem cells compared to myoblasts, Mol. Ther. 12 (2005) 1130–1141.

[6] T.R. Payne, H. Oshima, T. Sakai, Y. Ling, B. Gharaibeh, J. Cummins, J. Huard, Regeneration of dystrophin-expressing myocytes in the mdx heart by skeletal muscle stem cells, Gene Ther. 12 (2005) 1264–1274.

[7] T. Tamaki, A. Akatsuka, K. Ando, Y. Nakamura, H. Matsuzawa, T. Hotta, R.R. Roy, V.R. Edgerton, Identification of myogenic-endothelial progenitor cells in the interstitial spaces of skeletal muscle, J. Cell Biol. 157 (2002) 571–577.

[8] R. Sarig, Z. Baruchi, O. Fuchs, U. Nudel, D. Yaffe, Regeneration and transdifferentiation potential of muscle-derived stem cells propagated as myospheres, Stem Cells 24 (2006) 1769–1778.

[9] H. Gerhardt, C. Betsholtz, Endothelial-pericyte interactions in angiogenesis, Cell Tissue Res. 314 (2003) 15–23.

[10] L. da Silva Meirelles, P.C. Chagastelles, N.B. Nardi, Mesenchymal stem cells reside in virtually all post-natal organs and tissues, J. Cell Sci. 119 (2006) 2204–2213.

[11] M.F. Pittenger, B.J. Martin, Mesenchymal stem cells and their potential as cardiac therapeutics, Circ. Res. 95 (2004) 9–20.

[12] A. Sakamoto, K. Ono, M. Abe, G. Jasmin, T. Eki, Y. Murakami, T. Masaki, T. Toyo-oka, F. Hanaoka, Both hypertrophic and dilated cardiomyopathies are caused by mutation of the same gene, delta-sarcoglycan, in hamster: an animal model of disrupted dystrophin-associated glycoprotein complex, Proc. Natl. Acad. Sci. USA 94 (1997) 13873–13878.

[13] R. Coral-Vazquez, R.D. Cohn, S.A. Moore, J.A. Hill, R.M. Weiss, R.L. Davisson, V. Straub, R. Barresi, D. Bansal, R.F. Hrstka, R. Williamson, K.P. Campbell, Disruption of the sarcoglycan-sarcospan complex in vascular smooth muscle: a novel mechanism for cardiomyopathy and muscular dystrophy, Cell 98 (1999) 465–474.

[14] T. Shinagawa, S. Ishii, Generation of Ski-knockdown mice by expressing a long double-strand RNA from an RNA polymerase II promoter, Genes Dev. 17 (2003) 1340–1345.

[15] K.A. Lapidos, Y.E. Chen, J.U. Earley, A. Heydemann, J.M. Huber, M. Chien, A. Ma, E.M. McNally, Transplanted hematopoietic stem cells demonstrate impaired sarcoglycan expression after engraftment into cardiac and skeletal muscle, J. Clin. Invest. 114 (2004) 1577–1585.

[16] S. Noguchi, E. Wakabayashi, M. Imamura, M. Yoshida, E. Ozawa, Developmental expression of sarcoglycan gene products in cultured myocytes, Biochem. Biophys. Res. Commun. 262 (1999) 88–93.

[17] P. Vourc'h, M. Romero-Ramos, O. Chivatakarn, H.E. Young, P.A. Lucas, M. El-Kalay, M.F. Chesselet, Isolation and characterization of cells with neurogenic potential from adult skeletal muscle, Biochem. Biophys. Res. Commun. 317 (2004) 893–901.

[18] B. Brachvogel, H. Moch, F. Pausch, U. Schlotzer-Schrehardt, C. Hofmann, R. Hallmann, K. von der Mark, T. Winkler, E. Poschl, Perivascular cells expressing annexin A5 define a novel mesenchymal stem cell-like population with the capacity to differentiate into multiple mesenchymal lineages, Development 132 (2005) 2657–2668.

[19] G. Cossu, P. Bianco, Mesoangioblasts—vascular progenitors for extravascular mesodermal tissues, Curr. Opin. Genet. Dev. 13 (2003) 537–542.

[20] J. Pouly, A.A. Hagege, J.T. Vilquin, A. Bissery, A. Rouche, P. Bruneval, D. Duboc, M. Desnos, M. Fiszman, Y. Fromes, P. Menasche, Does the functional efficacy of skeletal myoblast transplantation extend to nonischemic cardiomyopathy? Circulation 110 (2004) 1626–1631.

[21] M.T. Wheeler, M.J. Allikian, A. Heydemann, M. Hadhazy, S. Zarnegar, E.M. McNally, Smooth muscle cell-extrinsic vascular spasm arises from cardiomyocyte degeneration in sarcoglycan-deficient cardiomyopathy, J. Clin. Invest. 113 (2004) 668–675.

[22] R. Fiaccavento, F. Carotenuto, M. Minieri, C. Fantini, G. Forte, A. Carbone, L. Carosella, R. Bei, L. Masuelli, C. Palumbo, A. Modesti, M. Prat, P. Di Nardo, Stem cell activation sustains hereditary hypertrophy in hamster cardiomyopathy, J. Pathol. 205 (2005) 397–407.

[23] A.T. Askari, S. Unzek, Z.B. Popovic, C.K. Goldman, F. Forudi, M. Kiedrowski, A. Rovner, S.G. Ellis, J.D. Thomas, P.E. DiCorleto, E.J. Topol, M.S. Penn, Effect of stromal-cell-derived factor 1 on stem-cell homing and tissue regeneration in ischaemic cardiomyopathy, Lancet 362 (2003) 697–703.

Available online at www.sciencedirect.com
ScienceDirect
Biochemical and Biophysical Research Communications 350 (2006) 1006–1012
BBRC
www.elsevier.com/locate/ybbrc

MicroRNA-1 facilitates skeletal myogenic differentiation without affecting osteoblastic and adipogenic differentiation

Norio Nakajima [a,b], Tomosaburo Takahashi [a,b,*], Ryoji Kitamura [a,b], Koji Isodono [a,b], Satoshi Asada [a,b], Tomomi Ueyama [b], Hiroaki Matsubara [a,b], Hidemasa Oh [b]

[a] Department of Cardiovascular Medicine, Kyoto Prefectural University of Medicine, Kyoto 602-8566, Japan
[b] Department of Experimental Therapeutics, Translational Research Center, Kyoto University Hospital, Kyoto 606-8507, Japan

Received 26 September 2006
Available online 6 October 2006

Abstract

MicroRNAs (miRNAs) are small non-coding RNAs emerging as important post-transcriptional gene regulators. In this study, we examined the role of miR-1, an miRNA specifically expressed in cardiac and skeletal muscle tissue, on the myogenic, osteoblastic, and adipogenic differentiation of C2C12 cells. Upon induction of myogenic differentiation, miR-1 was robustly expressed. Retrovirus-mediated overexpression of miR-1 markedly enhanced expression of muscle creatine kinase, sarcomeric myosin, and α-actinin, while the effects on myogenin and MyoD expression were modest. Formation of myotubes was significantly augmented in miR-1-overexpressing cells, indicating miR-1 expression enhanced not only myogenic differentiation but also maturation into myotubes. In contrast, osteoblastic and adipogenic differentiation was not affected by forced expression of miR-1. Thus, the muscle-specific miRNA, miR-1, plays important roles in controlling myogenic differentiation and maturation in lineage-committed cells, rather than functioning in fate determination.

Keywords: MicroRNA; Differentiation; Skeletal muscle cells; Adipocytes; Osteoblasts; C2C12 cells

MicroRNAs (miRNAs) are a class of small non-coding RNAs that play an important role in the post-transcriptional regulation of protein-coding gene expression. They anneal to the complementary sequences in the 3'UTRs of target mRNAs and cause degradation or, more notably, translational inhibition of target transcripts [1]. Although the functions of only a handful of miRNAs have been identified, it is emerging that miRNAs are involved in a wide variety of biological functions such as developmental patterning, lineage differentiation, cell death, proliferation, insulin secretion, and antiviral defense [2]. MiRNA-1 (miR-1) is an miRNA that is specifically expressed in cardiac and skeletal muscle [3]. Transfection of miR-1 in HeLa cells, a human epithelial cell line, has been shown to shift the gene expression profile toward that of muscle cells [4]. It has also been shown that transgenic expression of miR-1 in mouse hearts results in a proliferation defect and a failure of cardiac myocyte expansion, suggesting premature differentiation of cardiac myocytes by miR-1 overexpression [3]. A recent study revealed that miR-1 promotes myogenesis of myoblasts while repressing proliferation [5], although only relatively early steps of myoblast differentiation were examined in this study. These studies suggest that miR-1 regulates the balance between differentiation and proliferation, but the roles of miR-1 in lineage specification and terminal differentiation remain to be clarified.

The C2C12 cell line is a subclone isolated from parental C2 cells established from the regenerating thigh muscle of an adult mouse. Although C2C12 cells are widely used as a myoblast cell line, these cells are also well characterized as mesenchymal progenitor cells, and can differentiate into several mesenchymal cell types including myocytes,

* Corresponding author. Fax: +81 75 251 5514.
E-mail address: ttaka@koto.kpu-m.ac.jp (T. Takahashi).

0006-291X/$ - see front matter © 2006 Elsevier Inc. All rights reserved.
doi:10.1016/j.bbrc.2006.09.153

osteoblasts, and adipocytes [6,7]. Incubation of C2C12 cells under low serum conditions induces muscle differentiation and fusion of cells into multinucleated myotubes. Treatment of C2C12 cells with bone morphogenetic protein (BMP)-2 blocks myotube formation and induces osteogenic differentiation instead [6,8,9]. Culturing the cells with adipogenic medium, treatment with long-chain fatty acids, or treatment with thiazolidinediones also blocks myotube formation and leads to typical adipocyte differentiation [7,10]. During differentiation into these cell types, the cells capture important aspects of their respective differentiation programs such as expression of tissue-specific transcription factors and functional gene products, providing unique opportunities to study the mechanisms of differentiation into these mesenchymal cell types.

Understanding the molecular mechanisms that control differentiation into various specialized types of cells is crucial not only for the advancement of stem or progenitor cell biology, but also for developing its clinical potential as a tissue regeneration therapy. Formation of specialized cells is a multistep process of specific cellular events that includes commitment into specific lineages, differentiation, and maturation. In this study, we used C2C12 cell differentiation as a model system to determine whether miR-1 plays a role in myogenic, osteoblastic, and adipogenic differentiation.

Materials and methods

Cell culture and differentiation induction. C2C12 cells (a kind gift from A. Takahashi) and 3T3-L1 cells (Japanese Collection of Research Bioresources) were maintained as described previously [11,12]. Myogenesis was induced by changing the growth medium to DMEM supplemented with 2% horse serum after the cells reached confluency [11]. Osteoblastic differentiation was induced by treating cells with 300 ng/ml recombinant human BMP-2 (Astellas Pharma) [13]. For adipogenic differentiation, the growth medium was switched to adipogenic induction medium for 3 days and subsequently to adipogenic maintenance medium for 7 days as described previously [10].

Northern blot analysis. Total RNA samples extracted using TRIZOL (Invitrogen) were electrophoresed on denaturing 15% polyacrylamide gels and electroblotted onto GeneScreen Plus membranes (Perkin-Elmer). The membranes were UV-crosslinked, baked, and hybridized with ^{32}P end-labeled oligonucleotide DNA probes in ULTRAhyb-Oligo (Ambion). After washing, hybridization signals were detected using the Bio-imaging analyzer system BAS5000 (Fuji Film). Mouse U6 was used as an internal control.

Immunofluorescent microscopy and quantitative analyses of myotubes. Cells were stained with an antibody against sarcomeric myosin (MF20; Developmental Studies Hybridoma Bank) followed by Alexa Fluor 555-conjugated anti-mouse IgG antibody (Invitrogen) with nuclear staining with DAPI. The average number of nuclei per myotube was determined by counting randomly chosen myosin-positive cells containing two or more nuclei, and 1000 nuclei per culture were counted. The fusion index was calculated as the ratio of the number of nuclei in myotubes with two or more nuclei to the total number of nuclei, and 5000 myotube nuclei were counted.

Oil red O staining and alkaline phosphatase (ALP) assays. Cells were fixed and stained with Oil Red O solution as described previously [12]. Oil Red O was eluted with 100% 2-propanol and measured at 490 nm absorbance for quantification. For ALP staining, cells were stained with a mixture of 0.01% (w/v) naphthol AS-MX phosphate and 0.25 mg/ml fast violet B salt (Sigma–Aldrich) and counterstained with Mayer's Hematoxylin Solution. ALP activity was determined with *p*-nitrophenyl phosphate as a substrate.

DNA constructs. To express miR-1 under the control of the U6 promoter, miR-1 precursor sequences were synthesized, annealed, and ligated into the pENTR/U6 vector (Invitrogen). An miR-1 expression plasmid under the control of the long terminal repeat of PCMV virus was constructed using genomic sequences of miR1-2 containing pre-miR-1 gene sequences with 50 bp flanking each side, and the pMSCV-puro vector (Clontech). For use as a control, a pMSCV-puro vector expressing EGFP was also made.

Retrovirus production and infection. GP2-293 cells were cotransfected with the envelop vector pVSV-G and pMSCV-puro vectors using FuGENE6 (Roche). The medium supernatant was collected and centrifuged to concentrate virus stocks according to the manufacturer's instruction. Cells were infected with the retrovirus in the presence of 4 μg/ml polybrene for 24 h, and the infected cells were selected with 2.5 μg/ml puromycin.

Reverse transcriptase (RT)-polymerase chain reaction (PCR). cDNA was synthesized and analyzed by kinetic real-time PCR using the ABI Prism 7700 Sequence Detector system (Applied Biosystems) with Platinum SYBR Green qPCR SuperMix (Invitrogen). Mouse β tubulin was used for normalization, and comparative threshold (C_T) method was used to assess relative abundance of the targets. Primers used were myogenin-f: TACGT CCATCGTGGACAGCAT, myogenin-r: TCAGCTAAATTCCCT CGCTGG; myoD-f: ACATAGACTTGACAGGCCCCGA, myoD-r: AGACCTTCGATGTAGCGGATGG; muscle creatine kinase (MCK)-f: CACCTCCACAGCACAGACAG, MCK-r: ACCTTGGCCATGTGAT TGTT; β-tubulin-f: GGAACATAGCCGTAAACTGC, β-tubulin-r: TCA CTGTGCCTGAACTTACC; osterix-f: GGGTTAAGGGGAGCAAAG TCAGAT, osterix-r: CTGGGGAAAGGAGGCACAAAGAAG; osteocalcin-f: CTGAGTCTGACAAAGCCTTC, osteocalcin-r: GCTGTGAC ATCCATACTTGC; ALP-f: AACCCAGACACAAGCATTCC, ALP-r: GCCTTTGAGGTTTTTGGTCA; PPARγ-f: CCCTGGCAAAGCA TTTGTAT, PPARγ-r: GAAACTGGCACCCTTGAAAA; C/EBPα-f: GAACAGCAACGAGTACCGGGTA, C/EBPα-r: GCCATGGCCTTG ACCAAGGAG; aP2-f: CCGCAGACGACAGGA, aP2-r: CTCATGC CCTTTCATAAACT.

Immunoblot analysis. Cell lysates containing equal amounts of protein were electrophoresed on 10% SDS–polyacrylamide gels and transferred to polyvinylidene difluoride membranes (Millipore). Blots were immunoblotted with the primary antibody against sarcomeric myosin, α-actinin (EA-53; Sigma–Aldrich) or α-tubulin (Sigma–Aldrich), and horseradish peroxidase-labeled donkey anti-mouse IgG as a secondary antibody, followed by enhanced chemiluminescence (GE Healthcare) [14].

Statistical analysis. All experiments were performed at least three times. Data were expressed as means ± standard error and analyzed by one-way ANOVA with post hoc analysis. A value of $P < 0.05$ was considered statistically significant.

Results and discussion

MiR-1 is a muscle-specific miRNA that is expressed during myogenic differentiation

We first examined the expression of miR-1 in C2C12 cells during differentiation into myocytes, osteoblasts, and adipocytes. Although myotube formation was completely abolished when cells were induced to differentiate into osteoblasts, myotube formation was evident upon adipogenic differentiation (Fig. 1A). In undifferentiated cells, miR-1 was not expressed, while its expression was robustly increased when cells were induced to differentiate into myotubes, but not into osteoblasts (Fig. 1B). MiR-1 expression was also observed upon adipogenic differentiation, which

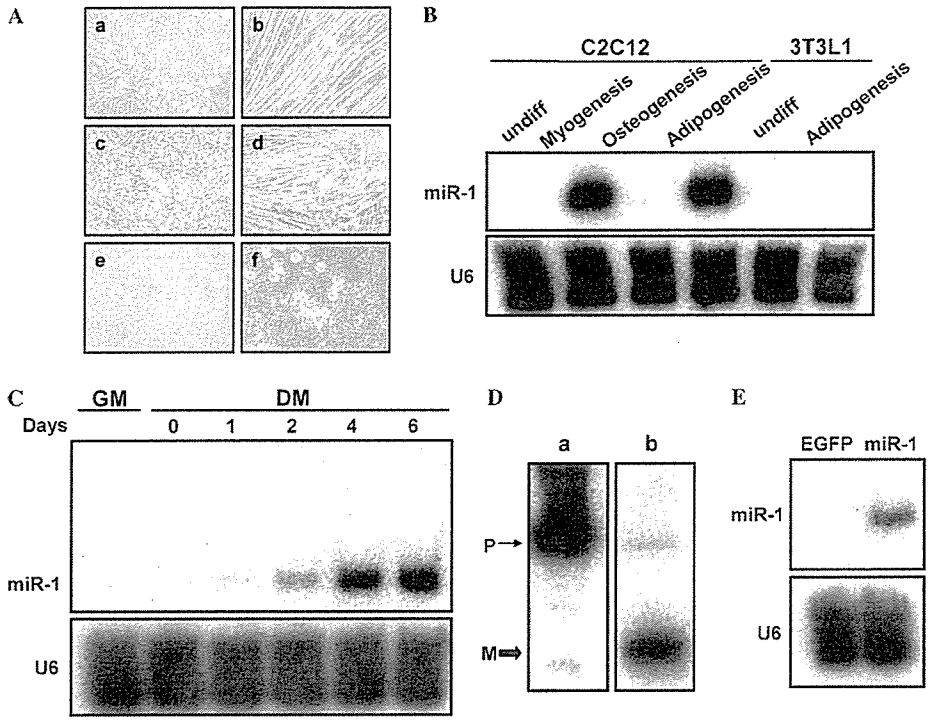

Fig. 1. MiR-1 is a muscle-specific miRNA that is expressed during myogenic differentiation. (A) Myogenic, osteoblastic, and adipogenic differentiation was induced in C2C12 cells (a–d) and 3T3-L1 cells (e,f). (a,e) Undifferentiated, (b) myogenic differentiation, (c) osteogenic differentiation, (d,f) adipogenic differentiation. (B) MiR-1 expression was analyzed in C2C12 cells or 3T3-L1 cells treated as indicated. (C) Myogenic differentiation was induced in C2C12 cells for the indicated periods of time (DM) or cells were cultured in growth medium (GM). Northern blot analysis was performed for miR-1 expression. (D) 293 cells were transfected with the pre-miR-1 (a) or the pri-miR-1-like molecule (b) expression vector, and miR-1 expression was analyzed. P, pre-miR-1; M, mature miR-1. (E) C2C12 cells were infected with EGFP or miR-1-expressing retrovirus vector, and miR-1 expression was analyzed. U6 was used as a loading control.

might reflect concomitant differentiation into myotubes in the adipogenic condition used in this study (Fig. 1A and B). MiR-1 expression was not observed in adipogenic differentiation of 3T3-L1 pre-adipocytes, where myotube formation was not observed (Fig. 1A and B). The observation that miR-1 expression was restricted to conditions that induced myotube formation was consistent with the previously observed restriction of miR-1 expression to cardiac and skeletal muscle in adult mice [3]. Kinetic analysis of miR-1 expression in myogenic differentiation revealed that miR-1 expression was readily detectable 2 days after induction of differentiation and reached its maximum at around days 4–6 (Fig. 1C). This time course correlated well with the expression of myogenic markers such as myogenin, a myogenic regulatory factor (MRF), and muscle type creatine kinase (MCK), a well-characterized marker for mature myocytes (Fig. 2), suggesting that miR-1 plays a role in controlling myogenic differentiation programs.

Overexpression of miR-1 facilitates myogenic differentiation

To analyze the role of miR-1 in C2C12 cell differentiation, we developed a vector-based expression system which efficiently expressed exogenous mature miR-1 in cells, since transient expression by synthetic RNA molecule transfection is not suitable for stable expression during the time course of C2C12 cell differentiation. When a precursor of miR-1 (pre-miR-1) was expressed under the control of the RNA polymerase III promoter, processing from the precursor to mature miR-1 was largely impaired, as revealed by much less abundance of mature miR-1 than pre-miR-1 (Fig. 1D). We then expressed a primary miR-1 (pri-miR-1) like molecule, consisting of the pre-miR-1 plus an additional 50 nucleotides taken from its genomic sequence on each end, under the control of the RNA polymerase II promoter. With this system, efficient expression of mature miR-1 was achieved (Fig. 1D), indicating that exogenous expression of pre-miR-1 is not sufficient for entering the proper processing mechanism, whereas expression of a pri-miR1-like molecule facilitates mature miR-1 expression. Therefore, we made a retroviral vector with this construct for efficient production of mature miR-1 in C2C12 cells (Fig. 1E).

Myogenic differentiation is a multistep dynamic process, during which the cells are defined to be myogenic (terminal commitment), differentiate into myocytes expressing muscle-specific structural and enzymatic proteins (biochemical differentiation), and subsequently fuse to form mature multinucleated myotubes (terminal differentiation). Progression through myogenic differentiation is controlled by

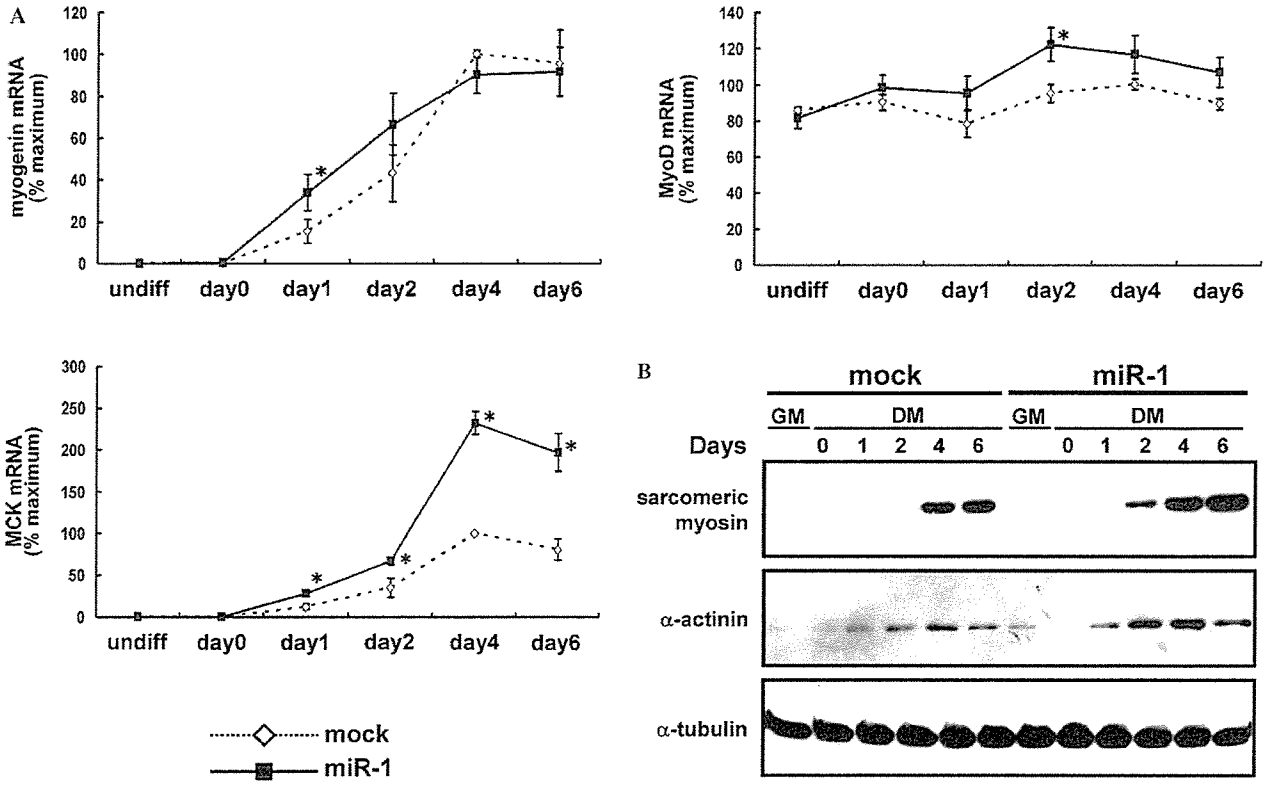

Fig. 2. Overexpression of miR-1 facilitates myogenic differentiation. Myogenic differentiation was induced for the indicated periods of time in C2C12 cells infected with mock or miR-1-expressing retrovirus. (A) Myogenin, MyoD, and MCK expression was analyzed with kinetic real-time PCR. The results were expressed as relative expression to β-tubulin and plotted as percentages of the maximum levels seen in mock-infected cells. $^*P < 0.05$ versus control. (B) Immunoblot analysis was performed using anti-sarcomeric myosin, anti-sarcomeric α-actinin, and anti-α-tubulin antibodies.

sequential activation of members of muscle-specific basic helix-loop-helix proteins called MRFs [15]. Among them, MyoD is expressed in undifferentiated myoblasts, while myogenin is activated during differentiation into myocytes. Myogenin expression in miR-1-overexpressing cells was accelerated at day 1, exhibiting a 2.1-fold increase in miR-1-overexpressing cells over mock-infected cells (Fig. 2A). A recent study [5] reported a similar observation, where the effect of transfection of a synthetic miR-1 duplex on myogenin expression was evaluated up to 24 h after induction of differentiation. Later time points were then examined with the aid of retrovirus-mediated stable expression of miR-1. Myogenin expression was comparable between miR-1-overexpressing cells and control cells after day 4, and a modest increase in MyoD expression was observed by miR-1 overexpression only in the differentiating state (Fig. 2A). However, a striking increase was observed in MCK expression in miR-1-overexpressing cells compared to mock-infected cells in the late phase (Fig. 2A). About a 2.7- and 3.8-fold enhancement in MCK expression in miR-1 cells was observed at day 4 and 6, respectively. Western blot analysis with anti-sarcomeric myosin and anti-sarcomeric α-actinin antibodies revealed that expression of these structural proteins was not only accelerated but also augmented by miR-1 overexpression (Fig. 2B). These results indicated that miR-1 overexpression enhanced the biochemical differentiation of myocytes.

MiR-1 overexpression leads to enhanced formation of multinucleated mature myotubes

Fusion of individual myocytes to form multinucleated mature myotubes is a unique feature of skeletal myogenic differentiation, and myoblast fusion has been shown to be regulated by mechanisms genetically dissociated from other myogenic processes such as biochemical differentiation [16–19]. Therefore, we analyzed the effect of miR-1 expression on the formation of mature myotubes and observed that in miR-1-overexpressing cells, myotubes were both higher in number and larger in size compared to mock-infected cells (Fig. 3A). This observation was quantified by the average number of nuclei per myotube (Fig. 3B), and by the percentage of all nuclei present in myotubes (fusion index) [20] (Fig. 3C). The results showed about a 1.9-fold increase in nuclei per myotube and a 1.6-fold increase in the fusion index.

Taken together, these results indicate that in addition to its role in the early steps of myogenic differentiation [5], miR-1 also plays an important role in late biochemical differentiation and in terminal differentiation. This was

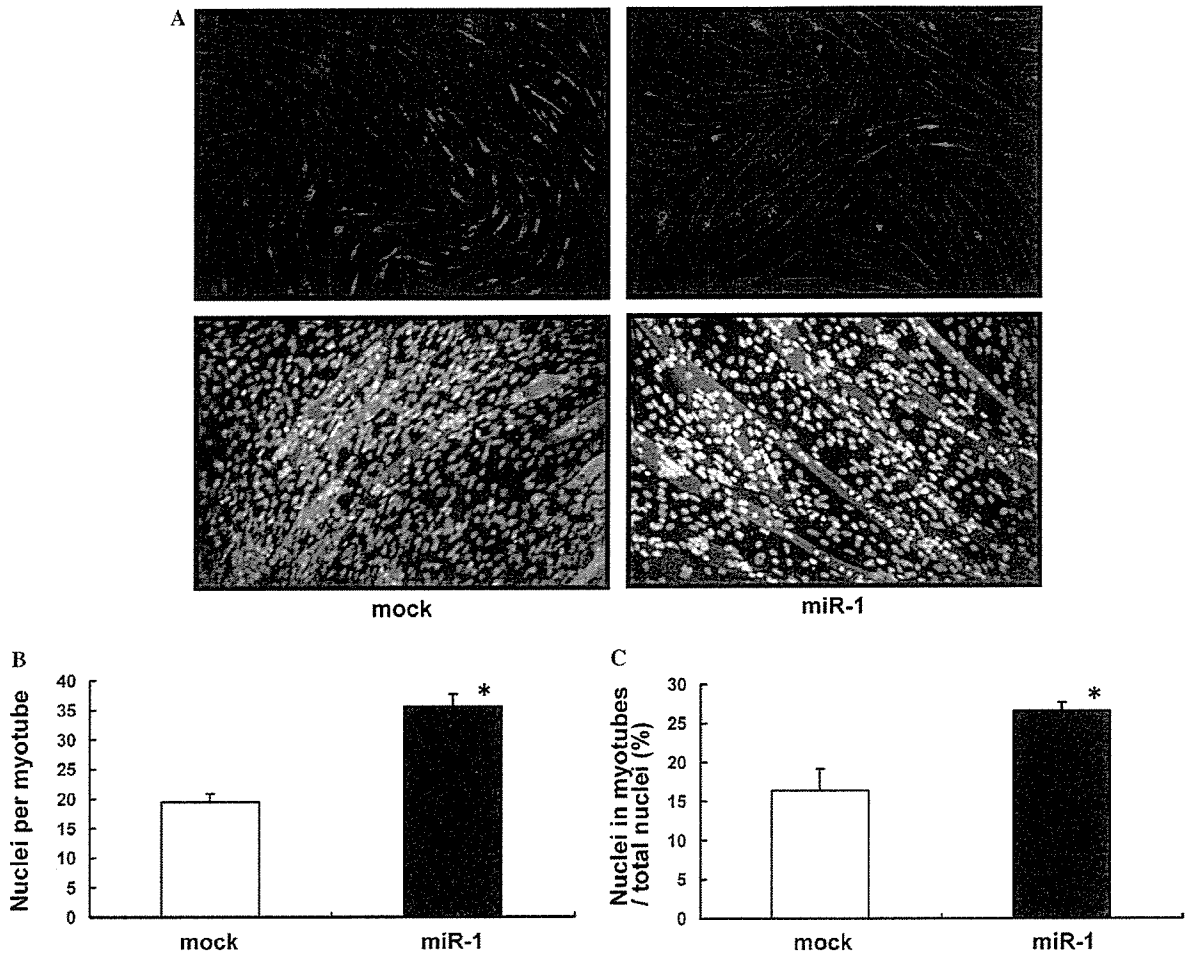

Fig. 3. MiR-1 overexpression leads to enhanced formation of multinucleated mature myotubes. Cells infected with mock or miR-1-expressing retrovirus were induced for myogenic differentiation for 6 days. (A) Myotubes were stained with anti-sarcomeric myosin antibody, and nuclei were stained with DAPI. (B) The mean number of nuclei per myotube was determined by counting 1000 nuclei per culture in three independent cultures. (C) The fusion index was defined as the ratio of nuclei within myotubes (cells containing two or more nuclei) to total number of nuclei, and percentages were plotted. Five thousand nuclei per culture were counted in three independent cultures. $^{*}P < 0.05$ versus control.

supported by: (i) the similar kinetics of endogenous miR-1 expression (Fig. 1C) with the expression of MCK, sarcomeric myosin, and α-actinin (Fig. 2A and B), and the formation of myotubes, which all peaked at days 4–6 after induction; and (ii) the enhancement of expression of mature myocyte markers and myotube fusion with overexpression of miR-1.

In the heart, which also endogenously expresses miR-1, it has been reported that overexpression of miR-1 in mouse hearts leads to a decrease in proliferating ventricular cardiac myocytes [3]. Although the role of miR-1 in the determination of myocyte fate could not be evaluated in this study, as a cardiac-specific β-myosin heavy chain promoter was used to drive miR-1 expression in cardiac myocytes, these results suggest that miR-1 expression in cardiac myocytes results in enhanced or premature differentiation of cardiac myocytes that impairs the balance between differentiation and proliferation. CHIP assays have demonstrated that MyoD and myogenin bind to regions upstream to miR-1 genes, suggesting these MRFs regulate expression of miR-1 [21]. These results with our observations suggested that miR-1 plays an important role in the relatively late stages of myogenic differentiation, although further studies are needed to fully clarify the functions of miR-1 in myogenesis.

MiR-1 does not influence osteoblastic or adipogenic differentiation

Since it is not known whether miR-1 plays a role in specification of cell fate to myogenic lineages, we analyzed the effects of miR-1 overexpression on the osteoblastic and adipogenic differentiation of C2C12 cells. The osteoblastic and adipogenic differentiation programs are also multistep processes [10,12,22,23], so we evaluated the expression of transcription factors involved in determination and initial differentiation of these lineages such as osterix, PPARγ, and C/EBPα, relatively late differentiation markers such

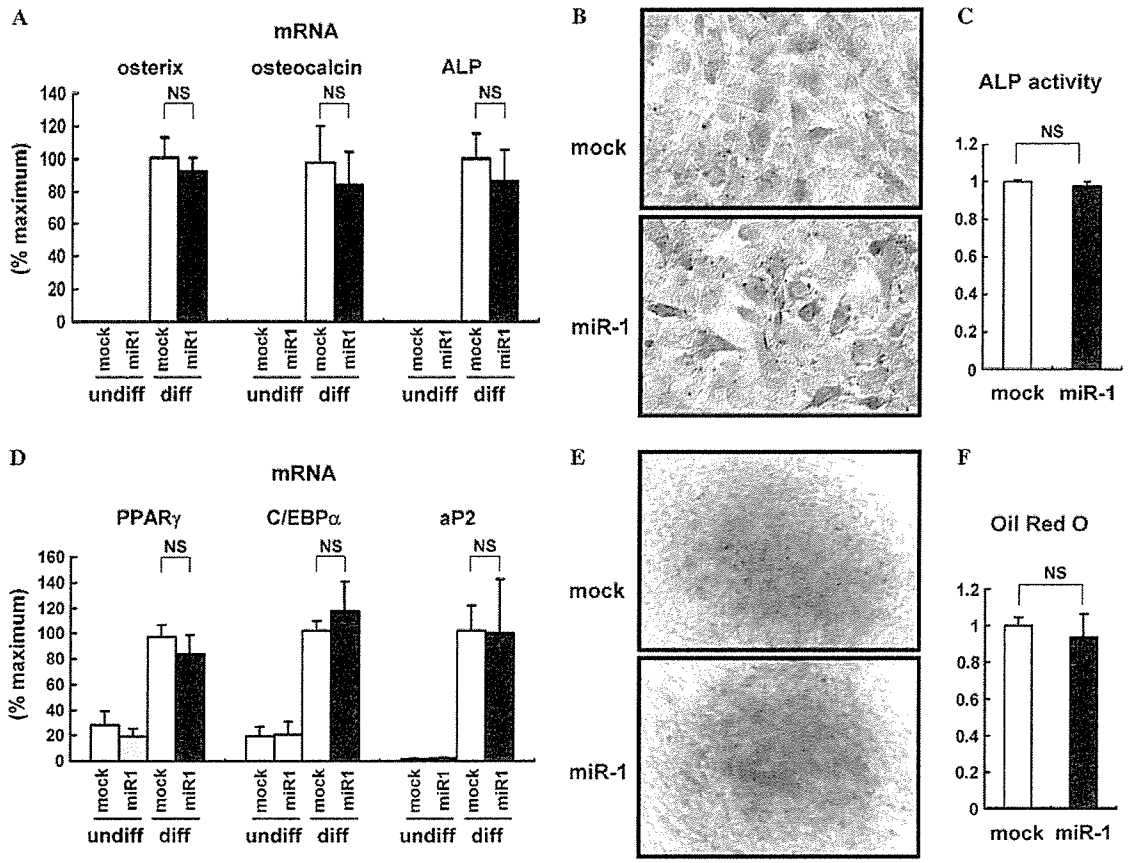

Fig. 4. MiR-1 does not influence osteoblastic or adipogenic differentiation. Osteoblastic (A–C) or adipogenic (D–F) differentiation was induced in mock-infected and miR-1-overexpressing C2C12 cells. (A) Osterix, osteocalcin, and ALP expression was measured by kinetic real-time PCR in undifferentiated and differentiated cells. (B) ALP staining was performed in differentiated cells. (C) ALP activity was determined with *p*-nitrophenyl phosphate as a substrate. (D) Kinetic PCR analysis was performed to analyze expression of PPARγ, C/EBPα, and aP2 in undifferentiated and differentiated cells. (E) Differentiated cells were stained with Oil Red O. (F) To quantify lipid accumulation, Oil Red O was extracted, and optical density was measured at 490 nm. NS; not significant.

as osteocalcin, ALP, and aP2, and characteristic biochemical features of these cells such as ALP activity and lipid accumulation. The osteoblastic markers osterix, osteocalcin, and ALP were absent in undifferentiated C2C12 cells, but markedly induced upon induction of osteoblastic differentiation (Fig. 4A). Neither the expression of these osteoblastic markers nor ALP staining and activity was altered by the exogenous expression of miR-1 during osteoblastic differentiation (Fig. 4A–C). When cells were cultured in adipogenic condition, adipogenic markers such as PPARγ, C/EBPα, and aP2 and lipid accumulation were significantly induced, and the forced expression of miR-1 did not alter the expression of these adipogenic marker genes or lipid accumulation in the cells (Fig. 4D–F). It has been reported that exogenous miR-1 expression in non-muscle cells shifts the mRNA expression profile towards muscle by downregulating the expression of genes not expressed in muscle [4]. Although these results suggested that miR-1 might act to prevent cells from differentiating into lineages other than muscle, our results showed that osteoblastic and adipogenic differentiation was not modulated by the expression of miR-1, implying that miR-1 does not function in determination of cell fate.

Conclusion

In this study, we analyzed the role of miR-1 in myogenic, osteoblastic, and adipogenic differentiation of C2C12 cells, and found that miR-1 enhanced myogenic differentiation and maturation into myotubes, but did not affect osteoblastic and adipogenic differentiation. These results suggest that miR-1 plays important roles in controlling the myogenic differentiation and maturation in lineage-committed cells, rather than functioning in fate determination. Identification of downstream targets of miR-1 will be an important issue to fully clarify the roles of miR-1 in myogenesis, which could be coordinately regulated by multiple miR-1 targets, since bioinformatic predictions indicate that each miRNA regulates on average ~200 target transcripts [24].

Acknowledgments

We thank Akihiro Takahashi for providing C2C12 cells, Astellas Pharma for BMP-2, Parth Patwari for critical reading of the manuscript, and Atsumi Kosugi and Mami Nishikawa for expert technical assistance. This work was supported by Grants-in-Aid from the Ministry of Education, Culture, Sports, Science and Technology of Japan, a grant from the Mitsubishi Pharma Research Foundation and Grants-in-Aid from the Ministry of Health, Labor, and Welfare of Japan.

References

[1] P.H. Olsen, V. Ambros, The *lin-4* regulatory RNA controls developmental timing in *Caenorhabditis elegans* by blocking LIN-14 protein synthesis after the initiation of translation, Dev. Biol. 216 (1999) 671–680.

[2] E. Wienholds, R.H.A. Plasterk, MicroRNA function in animal development, FEBS Lett. 579 (2005) 5911–5922.

[3] Y. Zhao, E. Samal, D. Srivastava, Serum response factor regulates a muscle-specific microRNA that targets *Hand2* during cardiogenesis, Nature 436 (2005) 214–220.

[4] L.P. Lim, N.C. Lau, P. Garrett-Engele, A. Grimson, J.M. Schelter, J. Castle, D.P. Bartel, P.S. Linsley, J.M. Johnson, Microarray analysis shows that some microRNAs downregulate large numbers of target mRNAs, Nature 433 (2005) 769–773.

[5] J.F. Chen, E.M. Mandel, J.M. Thomson, Q. Wu, T.E. Callis, S.M. Hammond, F.L. Conlon, D.Z. Wang, The role of microRNA-1 and microRNA-133 in skeletal muscle proliferation and differentiation, Nat. Genet. 38 (2006) 228–233.

[6] \T. Katagiri, A. Yamaguchi, M. Komaki, E. Abe, N. Takahashi, T. Ikeda, V. Rosen, J.M. Wozney, A. Fujisawa-Sehara, T. Suda, Bone morphogenetic protein-2 converts the differentiation pathway of C2C12 myoblasts into the osteoblast lineage, J. Cell Biol. 127 (1994) 1755–1766.

[7] L. Teboul, D. Gaillard, L. Staccini, H. Inadera, E.Z. Amri, P.A. Grimaldi, Thiazolidinediones and fatty acids convert myogenic cells into adipose-like cells, J. Biol. Chem. 270 (1995) 28183–28187.

[8] E. Chalaux, T. Lopez-Rovira, J.L. Rosa, R. Bartrons, F. Ventura, JunB is involved in the inhibition of myogenic differentiation by bone morphogenetic protein-2, J. Biol. Chem. 273 (1998) 537–543.

[9] D.S. de Jong, W.T. Steegenga, J.M. Hendriks, E.J. van Zoelen, W. Olijve, K.J. Dechering, Regulation of Notch signaling genes during BMP2-induced differentiation of osteoblast precursor cells, Biochem. Biophys. Res. Commun. 320 (2004) 100–107.

[10] T. Akimoto, T. Ushida, S. Miyaki, H. Akaogi, K. Tsuchiya, Z. Yan, R.S. Williams, T. Tateishi, Mechanical stretch inhibits myoblast-to-adipocyte differentiation through Wnt signaling, Biochem. Biophys. Res. Commun. 329 (2005) 381–385.

[11] A. Takahashi, Y. Kureishi, J. Yang, Z. Luo, K. Guo, D. Mukhopadhyay, Y. Ivashchenko, D. Branellec, K. Walsh, Myogenic Akt signaling regulates blood vessel recruitment during myofiber growth, Mol. Cell. Biol. 22 (2002) 4803–4814.

[12] J.B. Hansen, R.K. Petersen, B.M. Larsen, J. Bartkova, J. Alsner, K. Kristiansen, Activation of peroxisome proliferator-activated receptor γ bypasses the function of the retinoblastoma protein in adipocyte differentiation, J. Biol. Chem. 274 (1999) 2386–2393.

[13] Y. Lee, C. Ahn, J. Han, H. Choi, J. Kim, J. Yim, J. Lee, P. Provost, O. Radmark, S. Kim, V.N. Kim, The nuclear RNase III Drosha initiates microRNA processing, Nature 425 (2003) 415–419.

[14] T. Takahashi, B. Lord, P.C. Schulze, R.M. Fryer, S.S. Sarang, S.R. Gullans, R.T. Lee, Ascorbic acid enhances differentiation of embryonic stem cells into cardiac myocytes, Circulation 107 (2003) 1912–1916.

[15] M. Buckingham, L. Bajard, T. Chang, P. Daubas, J. Hadchouel, S. Meilhac, D. Montarras, D. Rocancourt, F. Relaix, The formation of skeletal muscle: from somite to limb, J. Anat. 202 (2003) 59–68.

[16] M. Crescenzi, D.H. Crouch, F. Tato, Transformation by myc prevents fusion but not biochemical differentiation of C2C12 myoblasts: mechanisms of phenotypic correction in mixed culture with normal cells, J. Cell Biol. 125 (1994) 1137–İ145.

[17] S. Russo, D. Tomatis, G. Collo, G. Tarone, F. Tato, Myogenic conversion of NIH3T3 cells by exogenous MyoD family members: dissociation of terminal differentiation from myotube formation, J. Cell Sci. 111 (1998) 691–700.

[18] I.H. Park, J. Chen, Mammalian target of rapamycin (mTOR) signaling is required for a late-stage fusion process during skeletal myotube maturation, J. Biol. Chem. 280 (2005) 32009–32017.

[19] A. Pisconti, S. Brunelli, M. Di Padova, C. De Palma, D. Deponti, S. Baesso, V. Sartorelli, G. Cossu, E. Clementi, Follistatin induction by nitric oxide through cyclic GMP: a tightly regulated signaling pathway that controls myoblast fusion, J. Cell Biol. 172 (2006) 233–244.

[20] V. Jacquemin, D. Furling, A. Bigot, G.S. Butler-Browne, V. Mouly, IGF-1 induces human myotube hypertrophy by increasing cell recruitment, Exp. Cell Res. 299 (2004) 148–158.

[21] P.K. Rao, R.M. Kumar, M. Farkhondeh, S. Baskerville, H.F. Lodish, Myogenic factors that regulate expression of muscle-specific microRNAs, Proc. Natl. Acad. Sci. USA 103 (2006) 8721–8726.

[22] A. Nakashima, T. Katagiri, M. Tamura, Cross-talk between Wnt and bone morphogenetic protein 2 (BMP-2) signaling in differentiation pathway of C2C12 myoblasts, J. Biol. Chem. 280 (2005) 37660–37668.

[23] Y.J. Kim, M.H. Lee, J.M. Wozney, J.Y. Cho, H.M. Ryoo, Bone morphogenetic protein-2-induced alkaline phosphatase expression is stimulated by Dlx5 and repressed by Msx2, J. Biol. Chem. 279 (2004) 50773–50780.

[24] A. Krek, D. Grun, M.N. Poy, R. Wolf, L. Rosenberg, E.J. Epstein, P. MacMenamin, I. da Piedade, K.C. Gunsalus, M. Stoffel, N. Rajewsky, Combinatorial microRNA target predictions, Nat. Genet. 37 (2005) 495–500.

Available online at www.sciencedirect.com
SCIENCE DIRECT
Journal of Molecular and Cellular Cardiology 40 (2006) 799–809
Journal of Molecular and Cellular Cardiology
www.elsevier.com/locate/yjmcc

Original article

Myocardium-targeted delivery of endothelial progenitor cells by ultrasound-mediated microbubble destruction improves cardiac function via an angiogenic response

Kan Zen [a], Mitsuhiko Okigaki [a,*], Yohei Hosokawa [b], Yasushi Adachi [c], Yoshihisa Nozawa [d], Michitaka Takamiya [a], Tetsuya Tatsumi [a], Norifumi Urao [a], Kento Tateishi [a], Tomosaburo Takahashi [a], Hiroaki Matsubara [a]

[a] *Department of Cardiovascular Medicine, Kyoto Prefectural University of Medicine, Kamigyo-ku, Kyoto, 602-8566, Japan*
[b] *Department of Pathology, Omihachiman City Hospital, Japan*
[c] *First Department of Pathology, Kansai Medical University, Japan*
[d] *Pharmacobioregulation Research Laboratory, Taiho Pharmaceutical Co. Ltd, Saitama, Japan*

Received 24 January 2006; accepted 14 March 2006
Available online 5 May 2006

Abstract

Application of ultrasound-mediated destruction of microbubbles (US + Bubble) to skeletal muscle creates capillary ruptures leading to leakage of the cell components. We studied whether US + Bubble combined with bone-marrow-derived mononuclear cells (BM-MNCs) infusion enables the targeted delivery of endothelial-lineage cells into the myocardium and improves cardiac function of the cardiomyopathy model due to the paucity of neocapillary formation. Pulsed US was applied to the anterior chest of BIOTO2 cardiomyopathy hamsters for 90 s after the intravenous injection of microbubble (Optison^{R}) followed by infusion of BM-MNCs. Cardiac samples from US + microbubble + BM-MNCs (US + Bubble + BM), US + Bubble, US + BM without Bubble, and saline infusion control groups were analyzed 12 weeks after treatment. Labeled BM-MNCs transplanted by US + Bubble were found to be mainly localized in the microvessels, but not by US stimulation without microbubble (121.2 ± 24.5 vs. 2.80 ± 1.30 cells/mm^2, $P < 0.001$). Capillary densities in US + Bubble + BM group were increased 1.7-fold ($P < 0.05$) over the control, and neither US + Bubble nor US + BM enhanced neocapillary formation. ^{99m}Tc-Tetrofosmin scintigraphy revealed that blood perfusion area in the US + Bubble + BM group was 48% greater than the control ($P < 0.01$). US + Bubble stimulation induces the expression of adhesion molecules (VCAM-1 and ICAM-1) in capillaries, and the US + Bubble-mediated supply of BM-MNCs increased the myocardial content of VEGF and bFGF. The left ventricular wt/body wt, area of cardiac fibrosis, and apoptotic cell numbers in the US + Bubble + BM group significantly ($P < 0.05$) decreased by 82%, 73%, and 64% relative to the control, respectively. The cardiac function in myopathic hamsters (assessed by fractional shortening) was markedly improved 36% ($P < 0.05$) by US + Bubble + BM treatment. Targeted delivery of BM-MNCs by US + Bubble to the myocardium of the cardiomyopathic hamster increased the capillary densities and regional blood flow and inhibited cardiac remodeling, resulting in the prevention of heart failure. This non-invasive cell delivery system may be useful as a novel efficient approach for angiogenic cell therapy to the myocardium.

Keywords: Angiogenesis; Endothelial progenitor; Ultrasound; Microbubble; Cardiomyopathy

1. Introduction

Cardiovascular diseases are often caused by a decrease in blood perfusion. Medical interventions to restore blood supply cannot be applied to all the patients. To treat those who are not candidates for conventional revascularization, alternative salvage therapy for neovascularization needs urgently to be developed. Recently, bone-marrow-derived endothelial progenitor cells (BM-EPCs) were isolated from the mononuclear cell (MNC) population in the peripheral blood [1,2]. These cells have a high proliferative activity and differentiated into ECs [2], suggesting that they may have the potential to accelerate neovascularization in the ischemic tissue. EPCs that were expanded from the adult peripheral or the cord blood

* Corresponding author. Fax: +81 75 251 5514.
E-mail address: okigakim@koto.kpu-m.ac.jp (M. Okigaki).

0022-2828/$ - see front matter © 2006 Elsevier Inc. All rights reserved.
doi:10.1016/j.yjmcc.2006.03.012

enabled the increase in the capillary density (CD) in the ischemic hindlimb [3,4]. Based on this basic research, the intramuscular transplantation of BM-MNCs has been clinically applied to induce angiogenesis in the ischemic limb [5]. Furthermore, clinical trials of catheter-based autologous BM-MNCs delivery approaches, intracoronary transfer for acute myocardial infarction [6–9], or intramyocardial injection for ischemic cardiomyopathy [10–12] resulted in an improvement of symptoms, blood perfusion, and function.

Besides obtaining diagnostic ultrasound (US) images, contrast agent microbubbles have been currently used for therapeutic purposes. US-mediated microbubble destruction in the capillary lumen elicits arteriogenesis and enhanced the hyperemic blood flow in normal [13] and ischemic [14] rat skeletal muscle. Microbubble destruction creates pores in the capillary walls, and this effect is dependent on the applied ultrasound power [13,15–17]. This method was applied to the targeted drug and gene delivery to the arterial vasculature [18,19] and tissue [20–23]. Targeted transfer of hepatocyte growth factor gene by US–microbubble destruction to cardiomyopathic hearts leads to the prevention of myocardial injury through angiogenesis actions [24,25].

Deterioration of cardiac function in the BIOTO2 cardiomyopathic hamster is attributed to a defect in δ-sarcoglycan that disrupts the dystrophin-associated glycoprotein complex, in which myocyte loss progresses in two ways. First, numerous vessel segments with constrictions and focal luminal narrowing develop. These vessel irregularities lead to focal ischemic injury and necrosis, resulting in myocyte loss [26]. Second, myocyte loss progresses owing to Ca^{2+} overload caused by high basal activity of Ca^{2+}-permeable channels or mechanosensitive Ca^{2+}-permeable channels [27]. In fact, Shimizu et al. [28] demonstrated the decreases in capillary numbers in the BIOTO2 myocardium by the histological examination and angiography using synchrotron radiation and concluded that impaired neoangiogenesis is involved in the progression of cardiac function in the BIOTO2. Furthermore, since Taniyama et al. reported that the angiogenetic gene therapy using hepatic growth factor (HGF) effectively increases the regional blood flow and prevents the progression of heart failure in the similar cardiomyopathic hamster BIO14.6 model [24]. Based on these previous findings, we attempted to study whether the increase in the regional blood perfusion by angiogenic cell therapy can prevent the progression of myocyte injury in the BIOTO2 hamster model.

The present study demonstrates that the intravenous infusion of BM-MNCs combined with US + Bubble enabled targeted delivery of BM-MNCs to the BIOTO2 myopathic hearts and induced the regional angiogenic response, resulting in an improvement of heart failure associated with the inhibition of cardiac remodeling and myocyte apoptosis. These findings suggest that this novel targeted cell delivery approach may be feasible as a non-invasive angiogenic cell therapy to the myocardium.

2. Materials and methods

2.1. Isolation of MNCs from the bone marrow

BM-MNCs were isolated by Percoll gradient centrifugation (Nycoprep, AXIS-SHIELD, Oslo, Norway) [29]. All animal experiments were approved by the Animal Care and Use Committee of Kyoto Prefectural University.

2.2. BM-MNCs delivery into the myocardium with microbubble–US

Eight-week-old BIOTO2 hamsters (Bio Breeders, Fitchburg, MA) were irradiated with low-frequency US (1 MHz, 50% duty ratio; ITO-US-3, Ito Co. Ltd, Tokyo, Japan) at an intensity of 2.0 W/cm^2 for 90 s, along with the intravenous injection of 200 μl microbubble (Optison, Mallincklodt Inc) and 300 μl saline, including 1×10^8 BM-MNCs. To prevent allograft rejection, recipients were administrated immunosuppressant FK-506 (1 mg/kg/day; Fujisawa Pharmaceutical Co., Osaka, Japan) using a mini-osmotic pump (Alzet 2004; Alza Co, Palo Alto, CA).

2.3. Tracking donor BM-MNCs

Donor BM-MNCs were labeled with 1,1′-dioctadecyl-3,3,3′,3′-tetramethylindocarbocyanine perchlorate (DiI, Molecular Probes, Inc) and infused to the recipient animals. After the indicated periods, hearts were frozen-sectioned and incubated with anti-von Willebrand factor (vWF) antibody (Santa Cruz Biotechnology, Inc, sc-8068) followed by FITC-conjugated secondary antibody. DiI+/vWF+ double-positive fluorescent cells were evaluated.

2.4. Histological and immunohistochemical analyses

Twelve weeks after BM-MNC delivery, the frozen-sectioned hearts were stained by alkaline phosphatase (ALP) with indoxyl tetrazolium to measure viable vessel densities in randomly selected, ten microscopic fields. The paraffin-sectioned samples were also stained with Hematoxylin–Eosin or Sirius red, and the area of cardiac muscle fiber and collagen content was evaluated, respectively. Apoptotic cardiomyocytes were evaluated in frozen-sectioned samples with an In situ Cell Death detection kit (Roche) with diaminobenzidine (DAB) and counterstained with 0.5% methyl green (Sigma). For VCAM-1, ICAM-1, interleukin 1-beta (IL-1β), tumor necrosis factor-alpha (TNF-α), monocyte chemoattractant protein-1 (MCP-1), and macrophage/monocyte immunostaining, we used the rat model as their anti-hamster antibodies were not available. Two days after US + Bubble treatment to the Wistar rats, the paraffin-sectioned hearts were immunostained by anti-rat VCAM-1 (Santa Cruz Biotechnology), ICAM-1 (ENDOGEN), IL-1β (Santa Cruz Biotechnology), TNF-α (Biosource), MCP-1 (Abcam), and CD68 (ED-1, Serotec) with DAB counterstained with Hematoxylin. The frozen-sectioned hearts were also immunostained with anti-FITC-conjugated rat VCAM-1 or anti-PE-conjugated rat vWF antibodies (BD Pharmingen). Double immunostaining using anti-rat VCAM-1 (horse radish peroxidase: brown) and anti-CD68 (alkaline phosphatase: red) antibodies with DAB and naphtol, respectively, was also performed.

2.5. Immunocytochemistry

1×10^5 BM-MNCs were primarily cultured on fibronectin-coated chamber slides (Becton Dickinson) for 7 days with EBM-2 medium supplemented with 5%FBS, EGM-2-MV-SingleQuots (Clonetics), and then incubated with 2.4 μl/ml of DiI-labeled acetylated LDL (Molecular Probes) and 10 ng/ml of BS-1-FITC (Sigma). The double-stained cells were counted as EPCs.

2.6. Western blot and real-time polymerase chain reaction (PCR) analysis

At the indicated period after BM-MNCs infusion, the hamster LV lysates were subjected to Western blot analysis with antibodies against VCAM-1 and ICAM-1 (Santa Cruz Biotechnology) or antibodies against VEGF (R&D Systems) and basic FGF (Upstate), respectively, and visualized using an ECL detection kit (Amersham).

Two days after US + Bubble treatment to the Wistar rats, total RNA was extracted from LV and then the real-time PCR was performed using the commercial kit (QIAGEN). The IL-1β, TNF-α, and MCP-1 mRNA amounts in the US + Bubble-treated heart were compared with that of the non-treated group.

2.7. Monitoring cardiac blood flow with ^{99m}Tc-Tetrofosmin scintigraphy

Cardiac blood flow was evaluated with the ratio of cardiac uptaken to the total dosed radioactivity of ^{99m}Tc-Tetrofosmin. The frozen short-axis-sectioned hearts (50 μm thickness) at the mid-ventricle level were exposed to an imaging plate, and a radioactive image was obtained using a Bio Imaging Analysis System (FUJI Photo Film).

2.8. Evaluation of the ventricular dimension and function by echocardiography

Transthoracic M-mode echocardiogram (SONOS 5500; Hewlett-Packard) was obtained by the parasternal short axis at mid-papillary muscle levels, and the LV end-diastolic dimension (LVDd) and percent fractional shortening (%FS) were determined.

2.9. Statistics

Statistical analyses were performed with one-way ANOVA followed by pair-wise contrasts using Dunnett's test. Data

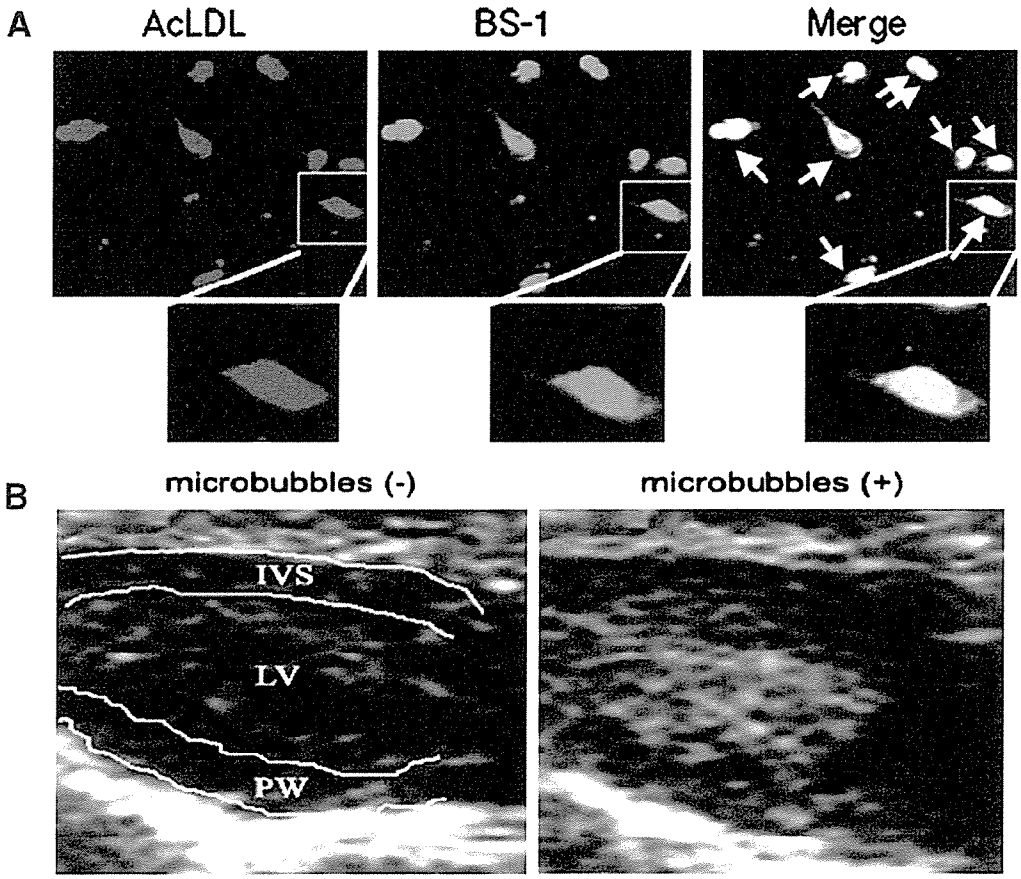

Fig. 1. EPC properties of BM-MNCs and the echocardiographic microbubble image. (A) BM-MNCs were cultured on fibronectin-coated plates for 7 days, and their binding ability to FITC-BS-1-Lectin and uptake of DiI-AcLDL was examined. BS-1+/AcLDL+ double fluorescent cells (arrows) in the merged image are considered to be the endothelial-lineage cells that exhibit a spindle shape. (B) The echocardiographical image (arrows) of microbubble delivery into the LV cavity immediately after microbubble injection. LV: left ventricle, IVS: intra-ventricular septum, PW: posterior wall. Scale bar indicates 100 μm.

(means ± SE) were considered statistically significant when P was <0.05.

3. Results

3.1. Incidence of endothelial-lineage cells in BM-MNCs

Immunocytochemical analysis indicated that 76 ± 2% of 7-day-cultured BM-MNCs (prepared from the BIOTO2 hamster) incorporated DiI-AcLDL and bound FITC-BS-1 (n = 5), some of which exhibited a spindle shape (Fig. 1A), suggesting that endothelial-lineage cells were considered to be included in this fraction as reported [5,30].

3.2. Targeted delivery of BM-MNCs to the myocardium by ultrasound-mediated microbubble destruction

US was applied to the anterior chest for 90 s immediately after intravenous injection of microbubble (Optison^R) into the BIOTO2 hamster followed by infusion of DiI-labeled 1 × 10^8 BM-MNCs. Echocardiography confirmed that microbubble was actually delivered into the LV cavity a few seconds after injection (Fig. 1B).

The transfused DiI-positive BM-MNCs were detected in the myocardium 2 weeks after US + Bubble stimulation but barely detectable by the US treatment alone without microbubble injection (121.2 ± 24.5 vs. 2.8 ± 1.3 cells/mm^2, n = 10, P < 0.001) (Fig. 2A). The DiI-positive BM-MNCs were mostly merged with endothelial marker vWF-positive microvessels (the merge panel in Fig. 2A), while no DiI+ cells were merged in the cardiomyocytes immunostained by cardiac a-myosin heavy chain (data not shown). Interestingly, DiI+ BM-MNCs were found to be attaching onto the endothelium of the microvessel 2 days after US + bubble stimulation (Fig. 2B).

3.3. US + Bubble + BM-MNCs treatment increased the capillary density and prevented cardiac remodeling

Capillary densities (CD) were evaluated by counting ALP+ viable capillaries. We found that the CD of the 20-week-old BIOTO2 hamster were decreased (48 ± 3%, P < 0.005) than the normal (F1B) hamsters and the US + Bubble + BM treatment significantly (P < 0.01) increased the CD (Fig. 3A), whereas there was no significant difference in the CD/myocyte ratio between the treated and untreated BIOTO2 hamsters

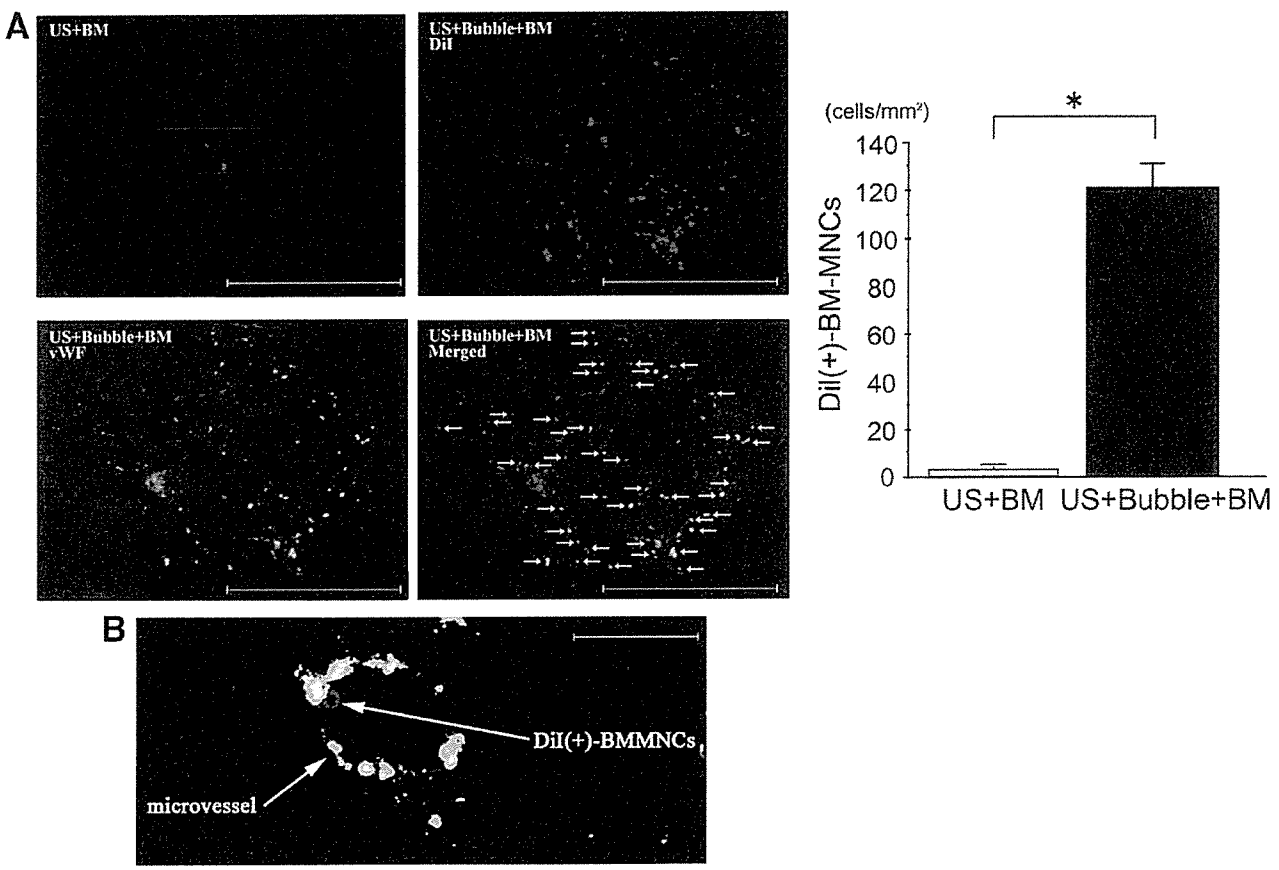

Fig. 2. Fluorescence micrograph of BM-MNCs transplanted by US + Microbubble. (A) US was applied to the anterior chest immediately after intravenous infusion of DiI-labeled BM-MNCs (1 × 10^8 cells) with microbubble (US + Bubble + BM) or without microbubble (US + BM). DiI+ BM-MNCs (red color) and vWF+ microvessels (green color) in the myocardial samples at 14 days after US + Bubble stimulation are shown. Calculated DiI+ cell numbers were significantly higher in US + Bubble + BM group than that in US + BM group (n = 10, *P < 0.001). DiI+ cells mostly corresponded to vWF+ microvessels in the merged image (arrows). Scale bars indicate 200 μm. (B) Attachment of DiI+ BM-MNCs onto the endothelial layer of the microvessel 2 days after US + bubble stimulation. Scale bar indicates 20 μm.

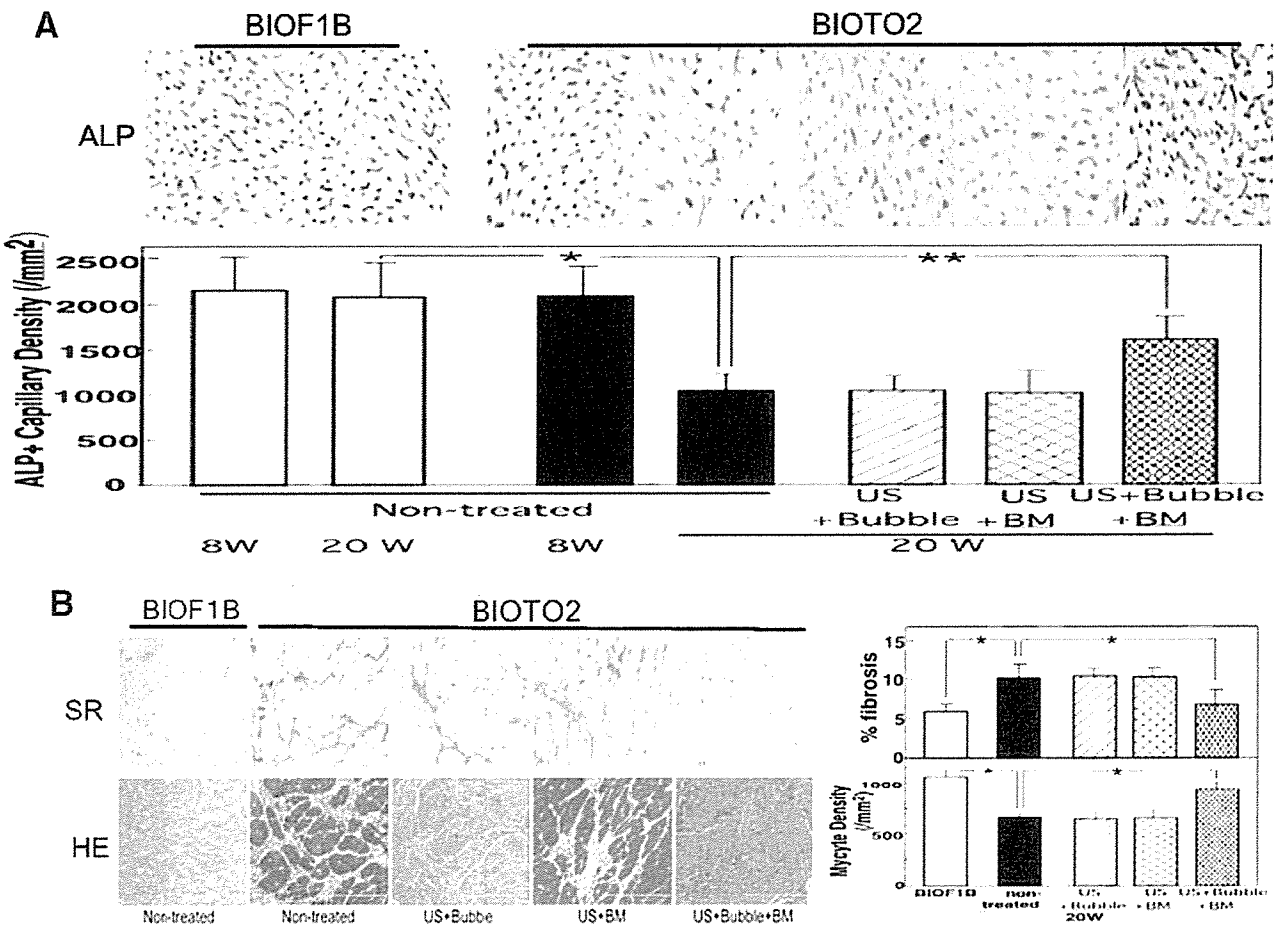

Fig. 3. Histological analysis of myopathic hearts treated with US + microbubble. (A) Evaluation of the capillary density (CD): 8-week-old hamsters were treated with US + microbubble + BM-MNCs infusion (US + Bubble + BM) ($n = 12$), US + microbubble (US + Bubble) ($n = 5$), and US + BM-MNC infusion (US + BM) ($n = 5$) or non-treated ($n = 10$). The LVs of 8- and 20-week-old BIOTO2 or control (BIOF1B) hamsters ($n = 6$) were frozen-sectioned and stained for alkaline phosphatase (ALP), and the number of ALP+ capillaries (blue dots) was counted. Representative images and statistical analysis were shown. $^{*}P < 0.005$, $^{**}P < 0.01$. (B) Evaluation of the cardiac fibrosis and myocyte density: LVs were frozen-sectioned or paraffin-sectioned and stained for Sirius red (SR) or Hematoxylin–Eosin (HE), respectively. Collagen deposition is shown as red color area in SR, while the muscle fibers were stained red in HE. Statistical analysis of the percent fibrosis (fibrotic area ratio to a total microscopic field) and the myocyte density is presented. $^{*}P < 0.01$. Scale bars in panels A and B indicate 200 μm.

(US + Bubble: 1.45 ± 0.15, US + BM: 1.52 ± 0.09, US + Bubble + BM: 1.46 ± 0.08, non-treated: 1.49 ± 0.08, $n = 6$ each). The decrease in myocyte densities in the untreated BIOTO2 hamsters relative to the US + Bubble + BM-treated hamsters (Fig. 3B) may account for the lack of significant difference in the CD/myocyte ratio. The compensatory hypertrophy of remaining cardiomyocytes may be also involved in this discrepancy. Similar findings (the discrepancy between CD and CD/myocyte ratio) were previously reported in the BIOTO2 hamsters [28].

The cardiac fibrosis and myocyte density were evaluated by Sirius red (SR) and Hematoxylin–Eosin (HE) staining,

Table 1
Body weight, ventricular weight, and heart rate data at the age of 20 weeks

	BW (g)	LVW (mg)	LVW/BW (mg/g)	HR (beats/min)
Non-treated ($n = 10$)	99.40 ± 8.859	299.3 ± 12.49	3.037 ± 0.339	308.7 ± 27.11
US + Bubble ($n = 5$)	94.80 ± 4.147	294.8 ± 16.14	3.111 ± 0.158	318.6 ± 24.45
US + BM ($n = 5$)	96.00 ± 12.33	291.2 ± 21.63	3.074 ± 0.462	305.0 ± 28.32
BM + US + Bubble ($n = 12$)	103.7 ± 9.957	264.1 ± 15.15*,§,†	2.564 ± 0.236*,§,†	315.8 ± 25.59

Values are means ± SD; control = BIOTO2 treated with intravenous administration of BM-MNCs-free 0.9% saline solution; US + Bubble = BIOTO2 treated with only ultrasound irradiation with microbubble contrast agents administration; BM = BIOTO2 treated with intravenous administration of BM-MNCs without ultrasound irradiation nor microbubble contrast agents administration; BM + US + Bubble = BIOTO2 treated with intravenous administration of BM-MNCs with ultrasound irradiation under microbubble contrast agents administration; BM-MNCs = bone marrow mononuclear cells; BW = body weight; LVW = left ventricular weight; HR = heart rate.

$^{*}P < 0.05$ vs. control; $^{**}P < 0.01$ vs. control; $^{\S}P < 0.05$ vs. US; $^{\dagger}P < 0.05$ vs. BM.

respectively (Fig. 3B). Extensive cardiac fibrosis and the decrease in myocyte density were observed in the untreated myopathic BIOTO2 hamster, as previously described [28]. The fibrosis and myocyte density were significantly recovered 27% and 36% by the US + Bubble + BM treatment, respectively (Fig. 3B). The number of the apoptotic cells in the US + Bubble + BM group was 23% less than the non-treated control group (0.53 ± 0.12, n = 12 vs. 0.69 ± 0.01/mm^2, n = 10, $P < 0.01$). LV weight of myopathic hamsters treated by the US + Bubble + BM-MNCs was decreased ~17.5% ($P < 0.01$) compared with those in the non-treated control, US + Bubble alone or BM injection groups (Table 1). Thus, BM-MNCs transplanted by the US + Bubble stimulation enhance neovessel formation in myopathic hearts and inhibited the cardiac remodeling, including interstitial fibrosis and cell apoptosis.

3.4. Increase in blood perfusion improved the cardiac function in the US + Bubble + BM-treated heart

Regional blood perfusion was evaluated by ^{99m}Tc-Tetrofosmin scintigraphy (Fig. 4A). The ^{99m}Tc-Tetrofosmin uptake was decreased all over the untreated myopathic heart, whereas the distribution of radioactivity was homogenously increased in the US + Bubble + BM-MNC infusion group and the total dosed radioactivity (% uptake) of ^{99m}Tc-Tetrofosmin was 1.2-fold greater ($n = 5$, $P < 0.01$) than that in the non-treated group (Fig. 4A, right panel). Thus, US + Bubble + BM-MNC treatment was shown to actually increase the regional blood perfusion in the myopathic hamster heart.

To examine the in vivo consequence of improvement of myocardial blood perfusion by US + Bubble + BM-MNC treatment, we analyzed the cardiac function, LV diastolic

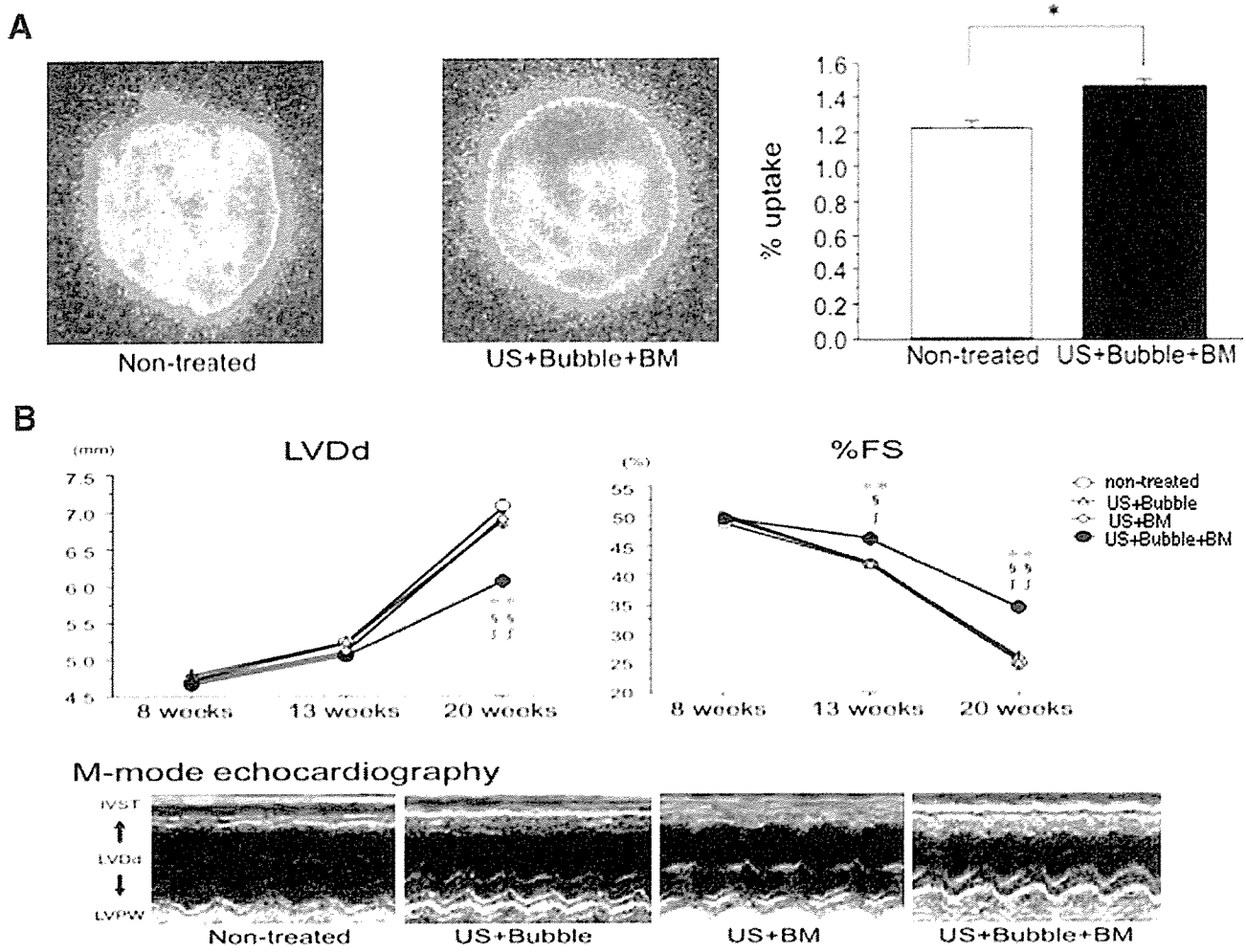

Fig. 4. Increase in blood perfusion improves the cardiac function of US + Bubble + BM-treated cardiomyopathy hamster. (A) Blood perfusion in the myocardium was evaluated by ^{99m}Tc-Tetrofosmin scintigraphy 12 weeks after US + microbubble + BM-MNCs infusion (US + Bubble + BM). Yellow and orange color indicate lower and higher blood perfusion, respectively. Myocardial ^{99m}Tc-Tetrofosmin uptake relative to the total dosed radioactivity (percent uptake) is evaluated in the right panel. The percent uptake was 1.2-fold higher ($n = 5$, $P < 0.01$) in the US + Bubble + BM-treated hamsters than in the non-treated group. $^{*}P < 0.01$ vs. non-treated control. (B) Evaluation of LV function by echocardiography. BIOTO2 hamsters (8-week-old) were treated with US + Bubble, US + BM, and US + Bubble + BM. LV functions were evaluated on Weeks 8, 13, and 20. Representative images on Week 20 are shown in the lower panel. The LV diastolic diameter (LVDd), fractional shortening (%FS), intra-ventricular septum (IVST), left ventricular posterior wall (LVPW), $^{**}P < 0.01$ vs. non-treated, $^{\S}P < 0.05$ vs. US + Bubble, $^{\S\S}P < 0.01$ vs. US + Bubble, $^{\dagger}P < 0.05$ vs. US + BM, $^{\dagger\dagger}P < 0.01$ vs. US + BM.

diameter (LVDd), and fractional shortening (%FS) by echocardiography on Weeks 8, 13, and 20 after treatment in the non-treated control, US + Bubble-, US + BM-MNCs-, and US + Bubble + BM-MNCs-treated groups (Fig. 4B). All parameters of Week 8 were not significantly different between each group. On Week 13, there were no significant differences in LVDd among each group, while %FS in the US + Bubble + BM-MNCs group was appreciably improved (11.1 ± 0.1%, $P < 0.05$) compared with the non-treated control, and the effect was more apparent at Week 20 (40.2 ± 0.2%, $P < 0.01$). At Week 20, the LVDd in the US + Bubble + BM-MNC group was also significantly improved over the control (18.4 ± 0.2%, $P < 0.01$). There were no changes in the LVDd and %FS between the non-treated control, US + Bubble, and US + BM-MNC treatment groups. Consistent with these parameters, the motion dynamics of the posterior wall and septum were apparently improved in US + Bubble + BM-MNC group (Fig. 4B, lower panel).

3.5. Expression of angiogenic growth factors by the transplanted BM-MNCs

We previously reported that BM-MNCs produce VEGF and bFGF that play a major role in the induction of neocapillary formation after BM-MNCs implantation into ischemic limbs [5,30] and myocardium [31]. We therefore examined the expression of VEGF and bFGF in the myopathic hearts in which BM-MNCs were transplanted by US + Bubble. Western blot analysis revealed that US + Bubble + BM-MNCs treatment markedly increased the expression of VEGF and bFGF ($P < 0.001$, 2.6-fold and 2.3-fold, respectively) compared with the non-treated control, while neither US + BM-MNCs nor the US + Bubble-treated groups showed significant changes (Fig. 5).

3.6. Induction of adhesion molecules and inflammatory cytokines by US + Bubble treatment

We next examined the possibility that US + Bubble treatment stimulates the expression of the adhesion molecules, causing the adhesion of transfused BM-MNCs or monocyte/macrophage onto the endothelial layer, as observed in Fig. 2B. Western blotting showed that the expressions of the adhesion molecules VCAM-1 and ICAM-1 increased to ~2.5-fold ($P < 0.01$) in the US + Bubble- or US + Bubbles + BM-MNCs-treated myocardium compared with the non-treated control, whereas only Bubble- or only US-treated groups did not induce the significant expression (Fig. 6A). To study the tissue localization of the adhesion molecules and monocyte/macrophages (CD68), we performed the immunohistochemical analysis. As the anti-hamster antibodies positive for VCAM-1, ICAM-1, and CD68 were not available, we prepared the rat myocardial samples 3 days after US + Bubble treatment and used the anti-rat antibodies for immunostaining. We found that the expressions of VCAM-1 and ICAM-1 were localized in the vWF+ vessels in the US + Bubble-treated myocardium (Fig. 6B, ICAM-1 not shown), whereas no expression was observed in the untreated

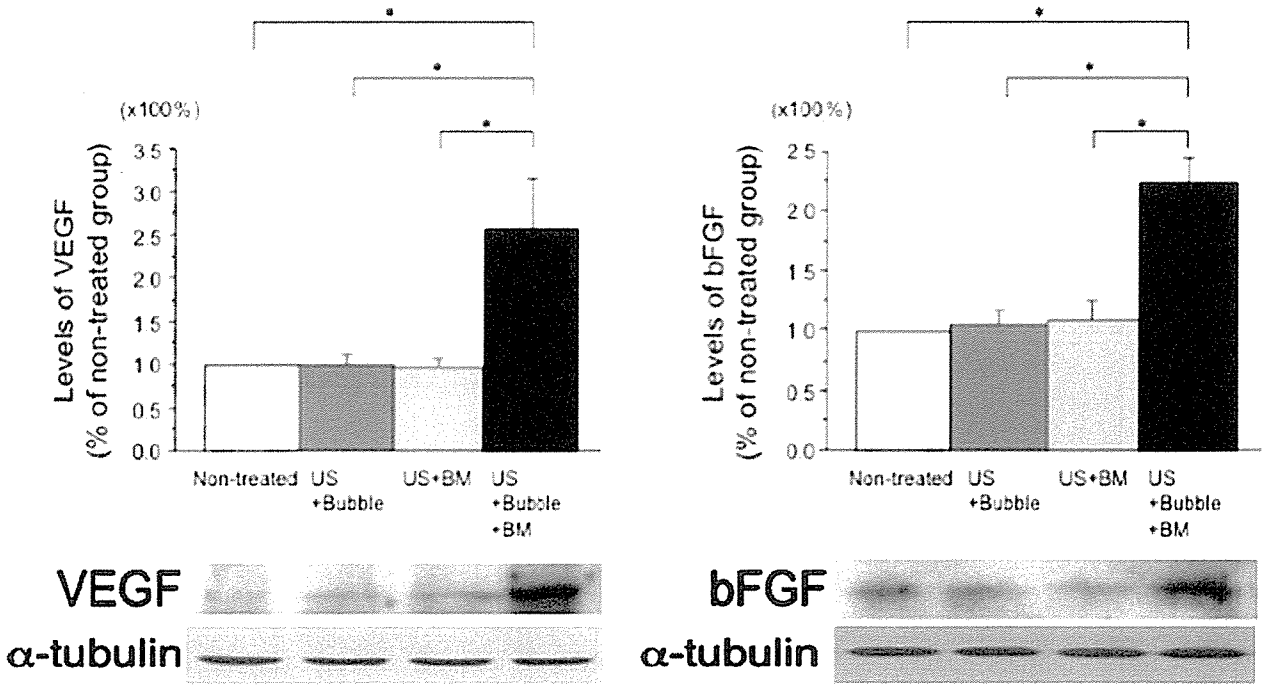

Fig. 5. Expression of angiogenic growth factors. Three days after US + BM, US + Bubble, or US + Bubble + BM treatment ($n = 5$, each), LV lysates were immunoblotted with the anti-VEGF, anti-basic FGF (bFGF), and anti-α-tubulin antibodies. The signal densities of VEGF and bFGF were arbitrarily normalized by that of α-tubulin. *$P < 0.001$.

control (Fig. 6C). The CD68+ macrophages were markedly infiltrated in the US + Bubble-treated myocardium (Fig. 6C, left panel), in which CD68+ cells mainly adhered onto the inner lumen of VCAM-1+ vessels and were partly observed in the interstitial region around the vessels (Fig. 6C, right panel), suggesting that the induction of the adhesion molecules in the US + Bubble-treated vessels caused the infiltration of macrophages into the interstitial region of myocardium.

We also examined the expression of TNF-α, IL-1β, and MCP-1 by the real-time PCR and immunohistochemical analysis. As the anti-hamster antibodies positive for MCP-1, TNF-α, and IL-1β were not available, we prepared the rat myocardial samples 3 days after US + Bubble treatment and used the anti-rat antibodies for immunostaining. The real-time PCR showed that their expressions are markedly elevated (approximately 7- to 15-fold, $P < 0.001$) compared with those in the non-treated control (Fig. 7A). The immunohistochemical analysis revealed that these cytokines (MCP-1, TNF-α, and IL-1β) were mainly expressed in the vessels in the US + Bubble-treated myocardium (Fig. 7B).

4. Discussion

A new delivery system of drugs or genes has been developed using US-targeted microbubble destruction. The drugs or genes that attach onto gas-filled microbubbles circulate through the intravascular space and are mechanically destroyed within the target organ by US [18,19,21,32], whereas no studies have been reported that determine whether this method is feasible for delivering the "vascular progenitor cells" to specific vascular sites. US-targeted microbubble destruction was reported to have an inflammatory action on

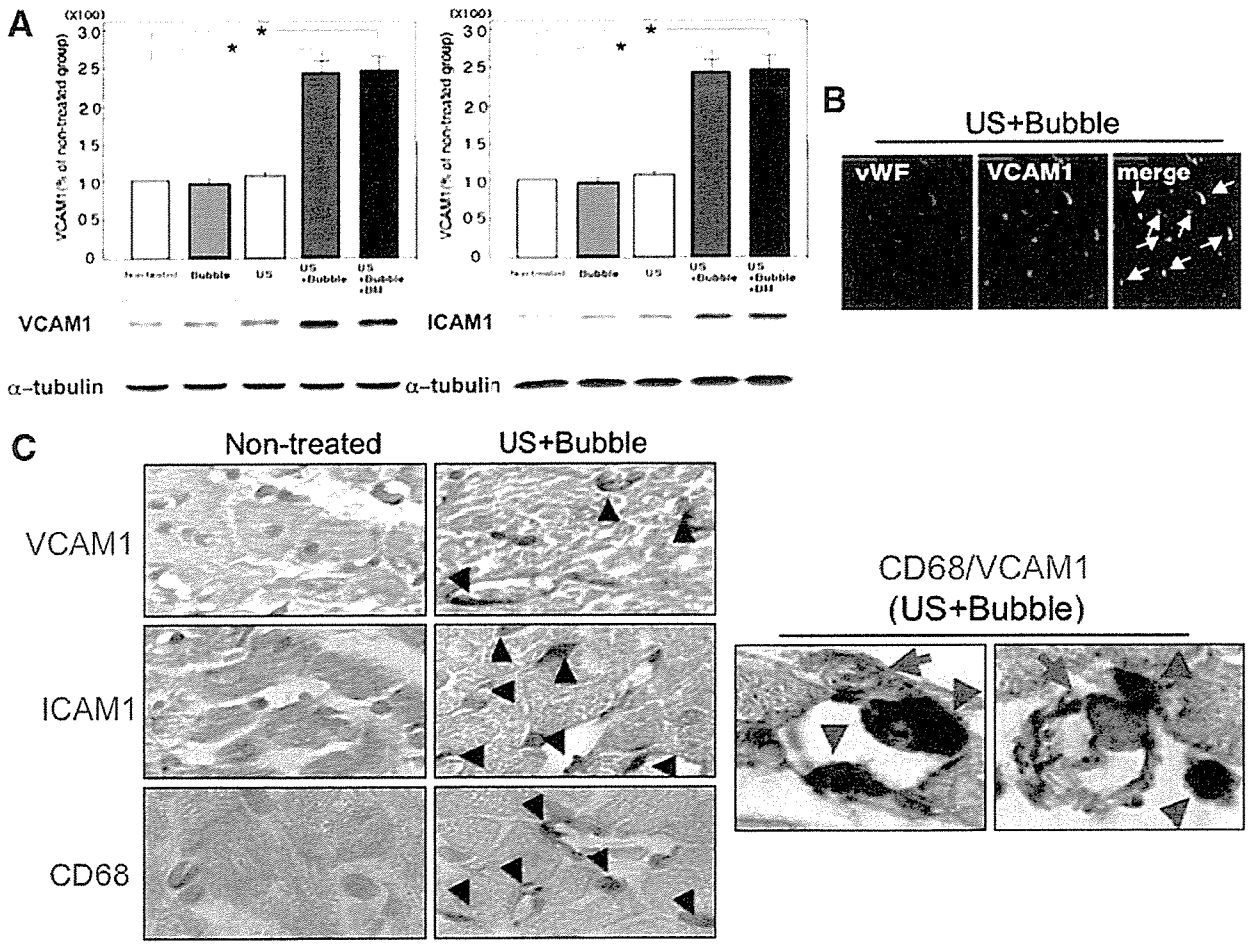

Fig. 6. Expression of adhesion molecules in US + Bubble-treated heart. (A) Two days after Bubble alone, US alone, US + Bubble, or US + Bubble + BM treatment, LV lysates were subjected to the immunoblot analysis using anti-VCAM-1, anti-ICAM-1, and anti-α-tubulin antibodies. Signal densities of VCAM-1 and ICAM-1 were arbitrarily normalized by α-tubulin. The expression of VCAM-1 and ICAM-1 was significantly ($*P < 0.01$) increased to 2.3- and 2.2-fold to compared the non-treated control, respectively. (B) For immunohistochemistry, we used the rat model as the hamster antibodies were not available. Frozen-sectioned rat LV samples (3 days after US + Bubble treatment) were immunostained with anti-rat vWF and anti-rat VCAM-1 antibodies followed by Rhodamin- or FITC-labeled secondary antibodies. VCAM-1 positive cells mostly corresponded to vWF positive vessels. Scale bar indicates 200 μm. (C) Two days after US + Bubble treatment, paraffin-sectioned rat LVs were immunostained using the antibodies against rat VCAM-1, ICAM-1, or CD68 (macrophage-specific antigen) with DAB or naphtol, respectively. Arrowheads in panel C, left panels indicate the VCAM-1+ or ICAM-1+ capillaries and CD68+ cells. Double fluorescence images using anti-rat CD68− and anti-rat VCAM-1− antibodies are presented in the right panels. CD68+ cells (red arrowheads) mainly adhered onto the inner lumen of VCAM-1+ vessels (brown arrows) or were partly observed in the interstitial region around the vessels.

the cell surface by making small holes that revert to a normal appearance within 24 h [13]. Song et al. [14,23] reported that US-targeted microbubble destruction causes capillary rupturing that stimulates neovessel formation and an increase in blood flow in both normal and ischemic skeletal muscles. We previously demonstrated that the recruitment of BM-MNCs stimulates angiogenesis in ischemic muscles by releasing angiogenic factors, including VEGF or bFGF and by the supply of endothelial progenitors [29,30]. Furthermore, we reported that BM-MNCs had a higher adhesive activity on the endothelium than did peripheral blood MNCs, and this adhesive activity was dependent on the expression level of adhesion molecules on the endothelium [29]. We therefore expanded the previous studies by Song et al. [14,23] and further studied whether US-mediated microbubble destruction, combined with the intravenous transfusion of BM-MNCs, enhanced neovessel formation by an increase in the endothelial attachment of BM-MNCs, leading to improvement in blood perfusion and cardiac function of BIOTO2 cardiomyopathy caused by limited neocapillary formation [26–28]. The present study demonstrates for the first time that this novel cell delivery system enables the vascular-endothelium-targeted attachment of infused BM-MNCs and increases the neovessel formation and blood flow in myopathic hearts, resulting in an improvement of cardiac function via the inhibition of myocyte apoptosis and interstitial fibrosis. This functional recovery was not found by BM-MNCs transfusion without US + Bubble, suggesting that US + Bubble-mediated BM-MNCs delivery is highly potent for neovascularization.

US + Bubble stimulation was reported to mechanically induce pores in the capillary wall [16]. The present study showed that the expression of adhesion molecules was markedly induced by the US + Bubble-mediated response (Fig. 5) and transfused BM-MNCs actually attached onto the injured endothelial layer (Fig. 2A). The adhesion activity of BM-MNCs on the endothelial layer was reported to be markedly higher than that of the circulating MNCs, and its adhesive activity was enhanced on the balloon-injured endothelium [29]. Indeed, as we observed in Fig. 2A, BM-MNCs infusion with US + Bubble stimulation achieved much more efficient regional cell delivery than simple BMC injection. Transplantation of autologous BM-MNCs has been clinically applied for patients with ischemic heart diseases via catheter-based approaches, direct injection into the ischemic myocardium [11,12,33], or intracoronary infusion [6–9]. Although they showed favorable effects on cardiac remodeling and function, the efficiency of cell delivery was still limited and such therapies were invasive. Most of the injected BM-derived mesenchymal stem cells died 4 days after intramyocardial injection [34], and ~60% of the BM-MNCs infused by intracoronary injection were trapped by the spleen and liver, and a minor population of cells (~10%) were present in the heart [35]. We only found a transient appearance of ventricular premature beats during the 90 s of US + Bubble application, and thereafter no incidences of death were observed during the observation period in any of the treated myopathic hamsters (n = 48). Thus, the present study suggests that US + Bubble + BM-MNC treatment is a

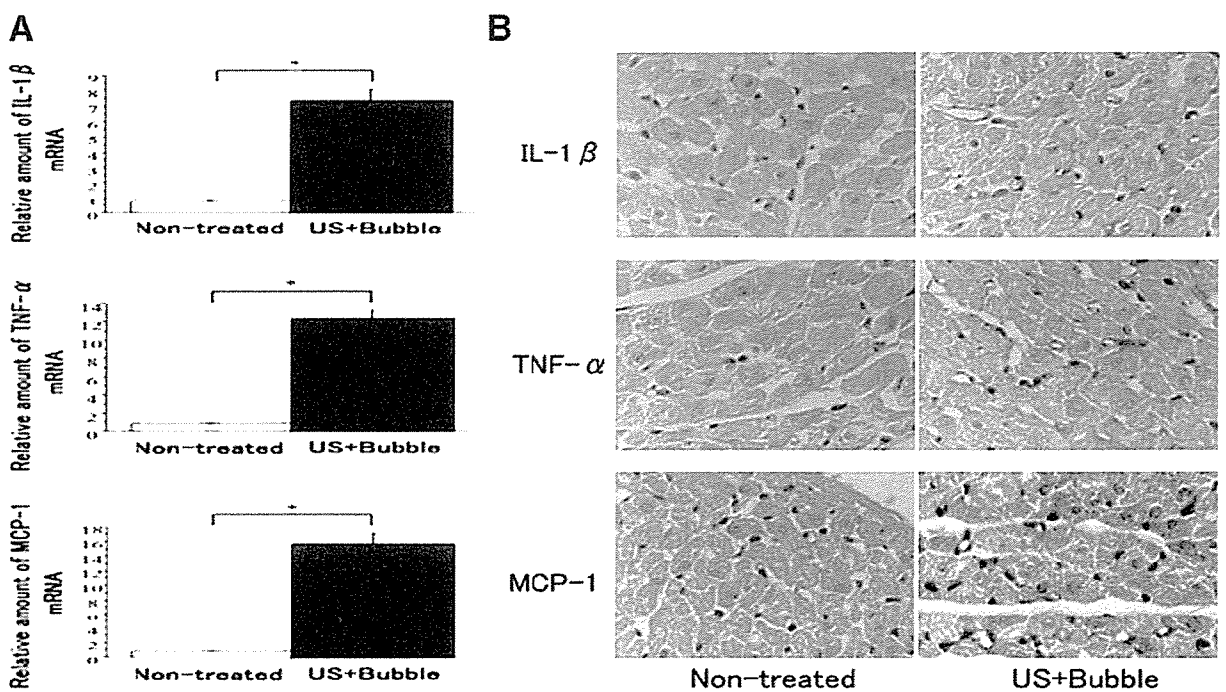

Fig. 7. US + Bubble induced the expression of inflammatory chemokine and cytokines. (A) Three days after US + Bubble treatment, total RNAs of rat LVs were subjected to the real-time PCR analysis for expression of IL-1β, TNF-α, and MCP1. Their mRNA levels in the US + Bubble-treated myocardium were significantly (*$P < 0.001$, $n = 5$ each) higher than those in the non-treated groups. (B) Rat LVs were also paraffin-sectioned and immunostained using the antibodies against rat IL-1β, rat TNF-α, and rat MCP-1. Brown dot indicates the positive cells.

safe and feasible non-invasive system for targeted cell delivery to the myocardium.

We found the adhesion of transfused BM-MNCs and the increased expressions of adhesion molecules on the US + Bubble-stimulated endothelium (Fig. 5). Considering our recent study reporting that systemically transplanted BM-MNCs can be firmly attached onto the injured vascular endothelium in an adhesive molecule-dependent manner [29], it is likely that the mechanical impact of US-mediated microbubble destruction induces the up-regulation of these adhesion molecules on the targeted vascular endothelium, causing the attachment of transfused BM-MNCs onto targeted endothelial layer. The present study clearly shows that endothelial progenitors included in BM-MNCs trans-differentiate to endothelial-like cells (Fig. 2) to repair US + Bubble-stimulated endothelium as well as supply the angiogenic factors (VEGF and bFGF) (Fig. 4) for neovessel formation. BM-MNC-derived endothelial progenitors that attached on the endothelial layer or leaked out from the injured endothelium may be incorporated into the regenerated endothelium and/or stimulate neovessel formation by supplying angiogenic factors. Thus, these synergistic bioeffects after US + Bubble + BM-MNC stimulation likely induced a potent angiogenic response in the US + microbubble-applied myocardium.

Although there is a concern that the US application to the anterior chest may cause the geometrical unevenness of the biological effects in the LV wall, there was no obvious difference in the biological effect between the anterior and the inferior LV wall in the US + Bubble + BM-treated heart, such as the CD (1354 ± 222.4 and 1288 ± 207.2/mm^2, n = 5) or the cardiac muscle fiber density (926.3 ± 88.7 and 901.3 ± 66.8/mm^2, n = 5). The diameter of the US probe (approximately 3 cm) is much bigger than the size of the hamster's heart (less than 1 cm), and furthermore the US was applied from various directions with continuously changing the angle to the chest wall, leading to achievement of the geometrically even biological effect all over the field of the myocardium.

The BIOTO2 Syrian hamsters used in this study inherit cardiomyopathy in an autosomal recessive manner and manifested dilated cardiomyopathy [36,37]. They have a genetic mutation of sarcoglycans, a subcomplex of the dystrophin-associated glycoprotein complex (DAGC) [38–40]. The impairment of the cardiac function in this hamster was caused by altered microvasculature, leading to a decrease in cardiac blood blow [26,28]. The BIOTO2 hamster exhibited a significantly lower capillary density [28] that correlated with the myocyte density and cardiac function. Angiogenetic gene therapy using hepatic growth factor was shown to enhance the angiogenic response and improve blood perfusion in the other myopathic hamster BIO14.6 model [24]. Combined with our present result using angiogenic cell therapy, it is likely that the enhancement of neovessel formation followed by an increase in regional blood flow inhibits cardiac remodeling in myopathic hearts and improves heart failure. Conclusively, BM-MNCs transplantation by US–microbubble-mediated cell delivery is a novel approach for an efficient angiogenic cell therapy, which is the most relevant strategy for the treatment of idiopathic myopathic hearts that requires an extensive cell delivery to the myocardium.

Acknowledgments

This study was supported in part by research grants from the Ministry of Education, Science, Sports and Culture, and the Ministry of Health, Labor and Welfare, Japan, the Study Group of Molecular Cardiology, the Japan Medical Association, and the Japan Heart Foundation.

References

[1] Asahara T, Murohara T, Sullivan A, Silver M, van der Zee R, Li T, et al. Isolation of putative progenitor endothelial cells for angiogenesis. Science 1997;275:964–7.

[2] Asahara T, Masuda H, Takahashi T, Kalka C, Pastore C, Silver M, et al. Bone marrow origin of endothelial progenitor cells responsible for postnatal vasculogenesis in physiological and pathological neovascularization. Circ Res 1999;85:221–8.

[3] Kalka C, Masuda H, Takahashi T, Kalka-Moll WM, Silver M, Kearney M, et al. Transplantation of ex vivo expanded endothelial progenitor cells for therapeutic neovascularization. Proc Natl Acad Sci U S A 2000; 97:3422–7.

[4] Murohara T, Ikeda H, Duan J, Shintani S, Sasaki K, Eguchi H, et al. Transplanted cord blood-derived endothelial precursor cells augment postnatal neovascularization. J Clin Invest 2000;105:1527–36.

[5] Tateishi-Yuyama E, Matsubara H, Murohara T, Ikeda U, Shintani S, Masaki H, et al, Therapeutic Angiogenesis using Cell Transplantation (TACT) Study Investigators. Therapeutic angiogenesis for patients with limb ischaemia by autologous transplantation of bone-marrow cells: a pilot study and a randomised controlled trial. Lancet 2002;360:427–35.

[6] Assmus B, Schachinger V, Teupe C, Britten M, Lehmann R, Dobert N, et al. Transplantation of progenitor cells and regeneration enhancement in acute myocardial infarction (TOPCARE-AMI). Circulation 2002;106: 3009–17.

[7] Britten MB, Abolmaali ND, Assmus B, Lehmann R, Honold J, Schmitt J, et al. Infarct remodeling after intracoronary progenitor cell treatment in patients with acute myocardial infarction (TOPCARE-AMI): mechanistic insights from serial contrast-enhanced magnetic resonance imaging. Circulation 2003;108:2212–8.

[8] Schachinger V, Assmus B, Britten MB, Honold J, Lehmann R, Teupe C, et al. Transplantation of progenitor cells and regeneration enhancement in acute myocardial infarction: final one-year results of the TOPCARE-AMI trial. J Am Coll Cardiol 2004;44:1690–9.

[9] Wollert KC, Meyer GP, Lotz J, Ringes-Lichtenberg S, Lippolt P, Breidenbach C, et al. Intracoronary autologous bone-marrow cell transfer after myocardial infarction: the BOOST randomised controlled clinical trial. Lancet 2004;364:141–8.

[10] Fuchs S, Satler LF, Kornowski R, Okubagzi P, Weisz G, Baffour R, et al. Catheter-based autologous bone marrow myocardial injection in no-option patients with advanced coronary artery disease: a feasibility study. J Am Coll Cardiol 2003;41:1721–4.

[11] Tse HF, Kwong YL, Chan JK, Lo G, Ho CL, Lau CP. Angiogenesis in ischaemic myocardium by intramyocardial autologous bone marrow mononuclear cell implantation. Lancet 2003;361:47–9.

[12] Perin EC, Dohmann HF, Borojevic R, Silva SA, Sousa AL, Mesquita CT, et al. Transendocardial, autologous bone marrow cell transplantation for severe, chronic ischemic heart failure. Circulation 2003;107:2294–302.

[13] Skyba DM, Price RJ, Linka AZ, Skalak TC, Kaul S. Direct in vivo visualization of intravascular destruction of microbubbles by ultrasound and its local effects on tissue. Circulation 1998;98:290–3.

[14] Song J, Cottler PS, Klibanov AL, Kaul S, Price RJ. Microvascular remodeling and accelerated hyperemia blood flow restoration in arterially

occluded skeletal muscle exposed to ultrasonic microbubble destruction. Am J Physiol, Heart Circ Physiol 2004;287:H2754–61.
[15] Price RJ, Skyba DM, Kaul S, Skalak TC. Delivery of colloidal particles and red blood cells to tissue through microvessel ruptures created by targeted microbubble destruction with ultrasound. Circulation 1998; 98:1264–7.
[16] Song J, Chappell JC, Qi M, VanGieson EJ, Kaul S, Price RJ. Influence of injection site, microvascular pressure, and ultrasound variables on microbubble-mediated delivery of microspheres to muscle. J Am Coll Cardiol 2002;39:726–31.
[17] Ay T, Havaux X, Van Camp G, Campanelli B, Gisellu G, Pasquet A, et al. Destruction of microbubbles by ultrasound: effects on myocardial function, coronary perfusion pressure, and microvascular integrity. Circulation 2001;104:461–6.
[18] Taniyama Y, Tachibana K, Hiraoka K, Namba T, Yamasaki K, Hashiya N, et al. Local delivery of plasmid DNA into rat carotid artery using ultrasound. Circulation 2002;105:1233–9.
[19] Teupe C, Richter S, Fisslthaler B, Randriamboavonjy V, Ihling C, Fleming I, et al. Vascular gene transfer of phosphomimetic endothelial nitric oxide synthase (S1177D) using ultrasound-enhanced destruction of plasmid-loaded microbubbles improves vasoreactivity. Circulation 2002;105:1104–9.
[20] Mukherjee D, Wong J, Griffin B, Ellis SG, Porter T, Sen S, et al. Ten-fold augmentation of endothelial uptake of vascular endothelial growth factor with ultrasound after systemic administration. J Am Coll Cardiol 2000; 35:1678–86.
[21] Price RJ, Kaul S. Contrast ultrasound targeted drug and gene delivery: an update on a new therapeutic modality. J Cardiovas Pharmacol Ther 2002;7:171–80.
[22] Shohet RV, Chen S, Zhou YT, Wang Z, Meidell RS, Unger RH, et al. Echocardiographic destruction of albumin microbubbles directs gene delivery to the myocardium. Circulation 2000;101:2554–6.
[23] Song J, Qi M, Kaul S, Price RJ. Stimulation of arteriogenesis in skeletal muscle by microbubble destruction with ultrasound. Circulation 2002; 106:1550–5.
[24] Taniyama Y, Morishita R, Aoki M, Hiraoka K, Yamasaki K, Hashiya N, et al. Angiogenesis and antifibrotic action by hepatocyte growth factor in cardiomyopathy. Hypertension 2002;40:47–53.
[25] Kondo I, Ohmori K, Oshita A, Takeuchi H, Fuke S, Shinomiya K, et al. Treatment of acute myocardial infarction by hepatocyte growth factor gene transfer: the first demonstration of myocardial transfer of a "functional" gene using ultrasonic microbubble destruction. J Am Coll Cardiol 2004;44:644–53.
[26] Factor SM, Minase T, Cho S, Dominitz R, Sonnenblick EH. Microvascular spasm in the cardiomyopathic Syrian hamster: a preventable cause of focal myocardial necrosis. Circulation 1982;66:342–54.
[27] Iwata Y, Katanōsaka Y, Arai Y, Komamura K, Miyatake K, Shigekawa M. A novel mechanism of myocyte degeneration involving the Ca^{2+}-permeable growth factor-regulated channel. J Cell Biol 2003;161:957–67.
[28] Shimizu T, Okamoto H, Watanabe M, Kumamoto H, Chiba S, Matsui Y, et al. Altered microvasculature is involved in remodeling processes in cardiomyopathic hamsters. Jpn Heart J 2003;44:111–26.
[29] Fujiyama S, Amano K, Uehira K, Yoshida M, Nishiwaki Y, Nozawa Y, et al. Bone marrow monocyte lineage cells adhere on injured endothelium in a monocyte chemoattractant protein-1-dependent manner and accelerate reendothelialization as endothelial progenitor cells. Circ Res 2003;93:980–9.
[30] Iba O, Matsubara H, Nozawa Y, Fujiyama S, Amano K, Mori Y, et al. Angiogenesis by implantation of peripheral blood mononuclear cells and platelets into ischemic limbs. Circulation 2002;106:2019–25.
[31] Kamihata H, Matsubara H, Nishiue T, Fujiyama S, Tsutsumi Y, Ozono R, et al. Implantation of bone marrow mononuclear cells into ischemic myocardium enhances collateral perfusion and regional function via side supply of angioblasts, angiogenic ligands, and cytokines. Circulation 2001;104:1046–52.
[32] Bekeredjian R, Chen S, Frenkel PA, Grayburn PA, Shohet RV. Ultrasound-targeted microbubble destruction can repeatedly direct highly specific plasmid expression to the heart. Circulation 2003;108:1022–6.
[33] Perin EC, Dohmann HF, Borojevic R, Silva SA, Sousa AL, Silva GV, et al. Improved exercise capacity and ischemia 6 and 12 months after transendocardial injection of autologous bone marrow mononuclear cells for ischemic cardiomyopathy. Circulation 2004;110(11 Suppl 1):II213–8.
[34] Toma C, Pittenger MF, Cahill KS, Byrne BJ, Kessler PD. Human mesenchymal stem cells differentiate to a cardiomyocyte phenotype in the adult murine heart. Circulation 2002;105:93–8.
[35] Siminiak T, Czepczynski R, Grygieska B, et al. Evidence for extravasation of intracoronary administered bone-marrow derived CD34+ stem cells in patients with acute myocardial infarction. Circulation 2004;110:III-51.
[36] Homburger F, Baker JR, Nixon CW, Wilgram G. New hereditary disease of Syrian hamsters. Primary, generalized polymyopathy and cardiac necrosis. Arch Intern Med 1962;110:660–2.
[37] Jasmin G, Eu HY. Cardiomyopathy of hamster dystrophy. Ann NY Acad Sci 1979;317:46–58.
[38] Roberds SL, Ervasti JM, Anderson RD, Ohlendieck K, Kahl SD, Zoloto D, et al. Disruption of the dystrophin–glycoprotein complex in the cardiomyopathic hamster. J Biol Chem 1993;268:11496–9.
[39] Sakamoto A, Ono K, Abe M, Jasmin G, Eki T, Murakami Y, et al. Both hypertrophic and dilated cardiomyopathies are caused by mutation of the same gene, -sarcoglycan, in hamster: an animal model of disrupted dystrophin-associated glycoprotein complex. Proc Natl Acad Sci U S A 1997;94:13873–8.
[40] Panchal BC, Trippodo NC. Systemic and regional haemodynamics in conscious Bio TO-2 cardiomyopathic hamsters. Cardiovasc Res 1993;27:2264–9.